



Claire C. Treatx and Anna-Maria Virkkala share first authorship. Invited review paper for the twentieth anniversary edition of *J. Geophysical Research-Biogeosciences* (published by AGU).

### Key Points:

- Rapid warming of northern permafrost region threatens ecosystems, soil carbon stocks, and global climate targets
- Long-term observations show importance of disturbance and cold season periods but are unable to detect spatiotemporal trends in C flux
- Combined modeling and syntheses show the permafrost region is a small terrestrial CO<sub>2</sub> sink with large spatial variability and net CH<sub>4</sub> source

### Supporting Information:

Supporting Information may be found in the online version of this article.

### Correspondence to:

C. C. Treat and A.-M. Virkkala,  
Claire.treat@awi.de;  
avirkkala@woodwellclimate.org

### Citation:

Treat, C. C., Virkkala, A.-M., Burke, E., Bruhwiler, L., Chatterjee, A., Fisher, J. B., et al. (2024). Permafrost carbon: Progress on understanding stocks and fluxes across northern terrestrial ecosystems. *Journal of Geophysical Research: Biogeosciences*, 129, e2023JG007638. <https://doi.org/10.1029/2023JG007638>

Received 13 OCT 2023

Accepted 7 FEB 2024

© 2024 The Authors.

This is an open access article under the terms of the [Creative Commons](#)

[Attribution-NonCommercial](#) License, which permits use, distribution and reproduction in any medium, provided the original work is properly cited and is not used for commercial purposes.

## Permafrost Carbon: Progress on Understanding Stocks and Fluxes Across Northern Terrestrial Ecosystems

Claire C. Treat<sup>1</sup> , Anna-Maria Virkkala<sup>2,3</sup>, Eleanor Burke<sup>4</sup> , Lori Bruhwiler<sup>5</sup> , Abhishek Chatterjee<sup>6</sup> , Joshua B. Fisher<sup>7</sup>, Josh Hashemi<sup>1</sup> , Frans-Jan W. Parmentier<sup>8,9</sup> , Brendan M. Rogers<sup>2</sup> , Sebastian Westermann<sup>8,9</sup> , Jennifer D. Watts<sup>2</sup> , Elena Blanc-Betes<sup>10</sup>, Matthias Fuchs<sup>11</sup>, Stefan Kruse<sup>12</sup> , Avni Malhotra<sup>13</sup>, Kimberley Miner<sup>6</sup>, Jens Strauss<sup>1</sup> , Amanda Armstrong<sup>14</sup>, Howard E. Epstein<sup>15</sup> , Bradley Gay<sup>6</sup> , Mathias Goeckede<sup>16</sup> , Aram Kalhor<sup>17</sup> , Dan Kou<sup>18</sup> , Charles E. Miller<sup>6</sup> , Susan M. Natali<sup>2</sup>, Youmi Oh<sup>5,19</sup>, Sarah Shakil<sup>20,21</sup> , Oliver Sonnenstag<sup>22</sup>, Ruth K. Varner<sup>23</sup> , Scott Zolkos<sup>2</sup>, Edward A.G. Schuur<sup>24</sup> , and Gustaf Hugelius<sup>3</sup>

<sup>1</sup>Permafrost Research Section, Alfred Wegener Institute Helmholtz Center for Polar and Marine Research, Potsdam, Germany, <sup>2</sup>Woodwell Climate Research Center, Falmouth, MA, USA, <sup>3</sup>Department of Physical Geography and Bolin Centre for Climate Research, Stockholm University, Stockholm, Sweden, <sup>4</sup>Met Office Hadley Centre, Exeter, UK, <sup>5</sup>NOAA Global Monitoring Laboratory, Boulder, CO, USA, <sup>6</sup>NASA Jet Propulsion Laboratory, California Institute of Technology, Pasadena, CA, USA, <sup>7</sup>Schmid College of Science and Technology, Chapman University, Orange, CA, USA, <sup>8</sup>Centre for Biogeochemistry in the Anthropocene, Department of Geosciences, University of Oslo, Oslo, Norway, <sup>9</sup>Department of Geosciences, University of Oslo, Oslo, Norway, <sup>10</sup>Institute for Sustainability, Energy and Environment, University of Illinois at Urbana-Champaign, Urbana, IL, USA, <sup>11</sup>Renewable and Sustainable Energy Institute, University of Colorado Boulder, Boulder, CO, USA, <sup>12</sup>Polar Terrestrial Environmental Systems, Alfred Wegener Institute Helmholtz Center for Polar and Marine Research, Potsdam, Germany, <sup>13</sup>Biological Sciences Division, Pacific Northwest National Laboratory, Richland, WA, USA, <sup>14</sup>University of Maryland Baltimore County - GESTAR 2, Baltimore, MD, USA, <sup>15</sup>Department of Environmental Sciences, University of Virginia, Charlottesville, VA, USA, <sup>16</sup>Department of Biogeochemical Signals, Max Planck Institute for Biogeochemistry, Jena, Germany, <sup>17</sup>GFZ German Research Centre for Geosciences, Potsdam, Germany, <sup>18</sup>Department of Biological and Environmental Sciences, Biogeochemistry Research Group, University of Eastern Finland, Kuopio, Finland, <sup>19</sup>Cooperative Institute for Research in Environmental Sciences, University of Colorado, Boulder, CO, USA, <sup>20</sup>Department of Biological Sciences, University of Alberta, Edmonton, AB, Canada, <sup>21</sup>Department of Ecology and Genetics, Limnology, Uppsala University, Uppsala, Sweden, <sup>22</sup>Département de géographie, Université de Montréal, Montréal, QC, Canada, <sup>23</sup>Department of Earth Sciences and Institute for the Study of Earth, Oceans and Space, University of New Hampshire, Durham, NH, USA, <sup>24</sup>Center for Ecosystem Science and Society, and Department of Biological Sciences, Northern Arizona University, Flagstaff, AZ, USA

**Abstract** Significant progress in permafrost carbon science made over the past decades include the identification of vast permafrost carbon stocks, the development of new pan-Arctic permafrost maps, an increase in terrestrial measurement sites for CO<sub>2</sub> and methane fluxes, and important factors affecting carbon cycling, including vegetation changes, periods of soil freezing and thawing, wildfire, and other disturbance events. Process-based modeling studies now include key elements of permafrost carbon cycling and advances in statistical modeling and inverse modeling enhance understanding of permafrost region C budgets. By combining existing data syntheses and model outputs, the permafrost region is likely a wetland methane source and small terrestrial ecosystem CO<sub>2</sub> sink with lower net CO<sub>2</sub> uptake toward higher latitudes, excluding wildfire emissions. For 2002–2014, the strongest CO<sub>2</sub> sink was located in western Canada (median:  $-52 \text{ g C m}^{-2} \text{ y}^{-1}$ ) and smallest sinks in Alaska, Canadian tundra, and Siberian tundra (medians:  $-5 \text{ to } -9 \text{ g C m}^{-2} \text{ y}^{-1}$ ). Eurasian regions had the largest median wetland methane fluxes ( $16\text{--}18 \text{ g CH}_4 \text{ m}^{-2} \text{ y}^{-1}$ ). Quantifying the regional scale carbon balance remains challenging because of high spatial and temporal variability and relatively low density of observations. More accurate permafrost region carbon fluxes require: (a) the development of better maps characterizing wetlands and dynamics of vegetation and disturbances, including abrupt permafrost thaw; (b) the establishment of new year-round CO<sub>2</sub> and methane flux sites in underrepresented areas; and (c) improved models that better represent important permafrost carbon cycle dynamics, including non-growing season emissions and disturbance effects.

**Plain Language Summary** Climate change and the consequent thawing of permafrost threatens to transform the permafrost region from a carbon sink into a carbon source, posing a challenge to global climate goals. Numerous studies over the past decades have identified important factors affecting carbon cycling,

including vegetation changes, periods of soil freezing and thawing, wildfire, and other disturbance events. Overall, studies show high wetland methane emissions and a small net carbon dioxide sink strength over the terrestrial permafrost region but results differ among modeling and upscaling approaches. Continued and coordinated efforts among field, modeling, and remote sensing communities are needed to integrate new knowledge from observations to modeling and predictions and finally to policy.

## 1. Introduction

The permafrost region covers approximately 15% of the land area in the northern hemisphere (Obu et al., 2019). The broad-scale distribution of permafrost on Earth is controlled by climate conditions, with the largest areas occurring in the Arctic and boreal regions, which are the focus of this study (Figure 1). Extensive permafrost is also found on the Tibetan plateau (Yang et al., 2010). Permafrost affects many aspects of ecosystem function, including hydrology, vegetation, and carbon and nutrient cycling (Schuur et al., 2008). Permafrost soils are often carbon (C) rich because cold and wet conditions limit microbial decomposition of organic material, allowing for the accumulation of a globally significant soil C stock (Hugelius et al., 2014; Strauss et al., 2021). However, climate warming is increasing soil temperatures (Biskaborn et al., 2019) and thawing permafrost (Nitze et al., 2018), enabling microbial transformation of some portion of these long-protected soil C stocks, contributing to greenhouse gas emissions and climate change (Schaefer et al., 2014; Schuur et al., 2015, 2022). However, there is large uncertainty in future climate projections with implications for international greenhouse gas emissions policy decisions (Natali et al., 2022).

Over the last 20 years, research on permafrost region C cycling and climate feedbacks has seen tremendous progress and growth (Sjöberg et al., 2020) through the integration of traditionally separate disciplines including ecology, soil science, biogeochemistry, atmospheric science, hydrology, geophysics, remote sensing, and modeling. In this paper, we synthesize current knowledge of permafrost ecosystem characteristics controlling C cycling as well as the measured and modeled terrestrial carbon dioxide ( $\text{CO}_2$ ) and methane ( $\text{CH}_4$ ) exchange between permafrost ecosystems and the atmosphere to identify next steps in understanding permafrost region C cycling.

### 1.1. Permafrost Region Overview: Extent and Characteristics

Permafrost is defined as subsurface earth material with temperature at or below  $0^\circ\text{C}$  for at least two consecutive years (Harris et al., 1988). Located between the ground surface and the continuously frozen permafrost, the “active layer” thaws and refreezes annually. Here, the majority of soil biological processes occur, including the formation and decomposition of soil organic matter. Permafrost occurs throughout the boreal, sub-Arctic and tundra landscapes (Figure 1). Within the broader climatic constraints of the permafrost domain, permafrost occurrence at a given site is moderated by local factors, such as slope and aspect, hydrology and soil moisture conditions, winter snow depth, vegetation cover, as well as the soil properties and ground ice (Shur & Jorgenson, 2007). These factors can vary considerably over distances of meters to kilometers, so areas with and without permafrost can coexist under similar climate. Additional key variables characterizing the state of permafrost include ground temperature, active layer thickness, ground ice content, and permafrost formation history (Jorgenson & Osterkamp, 2005; Osterkamp & Romanovsky, 1999; Romanovsky & Osterkamp, 2000; Shur et al., 2005; S. L. Smith et al., 2022).

The circum-Arctic permafrost region is often mapped as four regions: a continuous zone (90%–100% of land surface covered by permafrost), a discontinuous zone (50%–90% permafrost), a sporadic zone (10%–50%) and isolated (0%–10%) zone (Brown et al., 1998, revised 2001). Multiple new spatial data products for permafrost characteristics in the northern high latitudes are now available (Table 1). These products suggest relatively similar aerial extents for permafrost in the exposed land area ( $14$  and  $15.7 \times 10^6 \text{ km}^2$ ; Obu, 2021). If the entire permafrost region with its discontinuous zones without permafrost are considered, the permafrost region can cover up to  $23 \times 10^6 \text{ km}^2$  (Table 1); the Arctic-boreal permafrost domain, the focus of our review, covers  $18.4 \times 10^6 \text{ km}^2$  (Hugelius et al., 2023). Many permafrost maps largely build on the first permafrost map of the International Permafrost Association (IPA) (Brown et al., 1998, revised 2001). This was based on field mapping and manual digitizing of permafrost in different regions—a formidable effort that has not been repeated since. Most “modern”

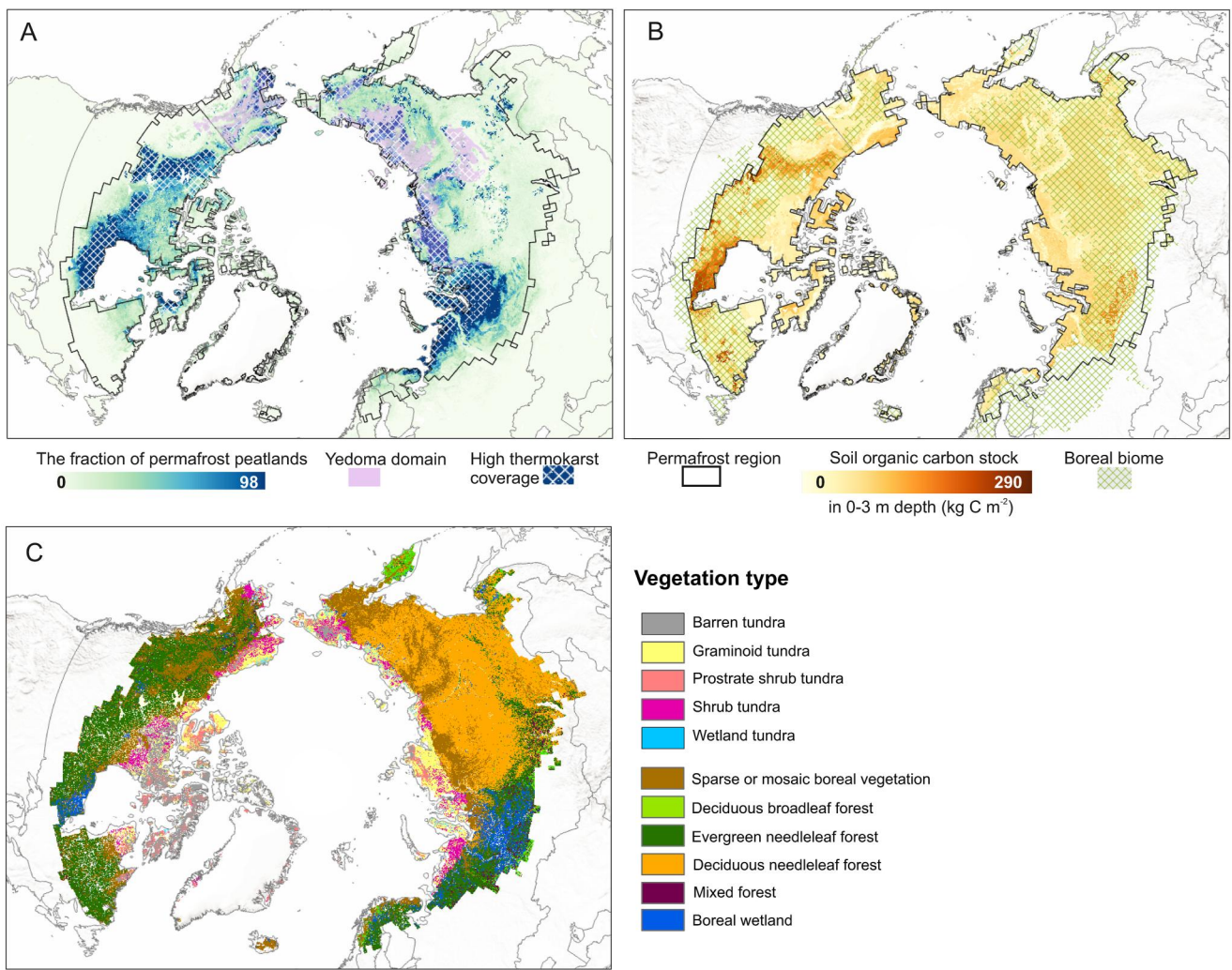


**Figure 1.** Maps showing (a) the permafrost peatland distribution (Hugelius et al., 2020), the distribution of Yedoma (purple; Strauss et al., 2022), landscapes with very high potential thermokarst coverage (Olefeldt et al., 2016), and (b) the distribution of the boreal biome and the soil organic carbon stocks within the permafrost region (Hugelius et al., 2014), and (c) vegetation types across the permafrost region following Virkkala et al., 2021 (note that the wetland extent on this map is likely underestimated). All maps also show the extent of the northern permafrost region as defined in the previous RECAPP-2 permafrost synthesis (Hugelius et al., 2023).

mapping approaches either rely on statistical relationships between climatic conditions and permafrost variables or on process-based models simulating ground thermal regimes (Obu et al., 2019; Ran et al., 2022). With such methods, gridded products of climate variables, such as air temperatures from climate re-analyses or remotely sensed land surface temperature, can be combined with geospatial data characterizing the landscape so that the effect of local factors on the ground thermal regime are better captured.

Permafrost maps are generally designed as “static” on timescales of several decades, and while useful to identify the spatial distribution of permafrost, the static concept is challenged by rapidly warming climate conditions in most permafrost areas (Rantanen et al., 2022). *In-situ* monitoring networks show increasing ground temperatures and a deepening of the active layer throughout most of the permafrost domain (Biskaborn et al., 2019; S. L. Smith et al., 2022). Furthermore, the formation of taliks, or the persistent unfrozen soil layer in a permafrost soil that forms when soils no longer freeze down to permafrost, is now widespread across Alaska (Farquharson et al., 2022). More abrupt disturbances such as retrogressive thaw slumps (mass movement and erosion on slopes), thermokarst lake and wetland formation, and thermokarst landscapes in general (i.e., land surface where the thawing of ice-rich permafrost terrain causes land subsidence) have been reported across all permafrost zones (Jorgenson et al., 2006; Nitze et al., 2018; Payette et al., 2004). Consequently, while the broad-scale extent and

**Table 1**

*Selected Spatial Circum-Polar Thematic (Permafrost, Soil) Map Products*

Theme	Study	Name	Description of approach	Spatial extent	Resolution	Type of map (vector/polygon, raster)
<i>Permafrost landscape characteristics and extent</i>						
Permafrost extent	Brown et al., 1998 revised 2001)	IPA Permafrost Map	Field mapping and manual digitalization	Pan-Arctic	12.5 km	Raster
Permafrost extent + zonation	Gruber (2012)		Equilibrium model using mean annual air temperature + terrain	Global	1 km	Raster
Permafrost extent	Obu et al. (2019)		TTOP Equilibrium temperature model + parameterization from satellite data	Pan-Arctic	1 km	Raster
Permafrost ground temperature and active layer thickness	Aalto et al. (2018)		Statistical modeling between ALT, climate data, and local environment	Land areas >30° N	1 km	Raster
Permafrost ground temperature, active layer thickness, zero annual amplitude	Ran et al. (2022)		Statistical modeling between ALT, climate data, local environment, soil characteristics	Pan-Arctic	1 km	Raster
Thermokarst landscape distribution	Olefeldt et al. (2016)		Data fusion product	Pan-Arctic	Polygons of variable size, with 28% of regions <1 ha and 13% > 1000 ha	Vector
Subsea permafrost	Overduin et al. (2019)	SuPerMAP	1-D transient heat flux accounting for sea level variation and sediments	Pan-Arctic; Arctic Ocean	12.5 km	
Ground ice type and abundance	O'Neill et al. (2019)		Data fusion model	Canada	1 km	Raster
<i>Permafrost region soils: characteristics, extent, C stocks</i>						
Yedoma domain extent	(Strauss et al., 2021)		Harmonized geological maps, remote sensing and Field mapping, including manual digitalization	Pan-Arctic	Polygons of variable size	Polygon
Peatland extent, depth, and C densities	Hugelius et al. (2020)		Harmonized soil maps and statistical modeling	North of 23°N	10 km	Raster
Soil class, soil properties, C density	Tarnocai et al. (2009)	NCSCD	Harmonized soil maps and statistical modeling	Permafrost region		Polygon
Soil class, soil properties, C density	Hugelius et al. (2013)	NCSCDv2.0	Harmonized soil maps and statistical modeling	Permafrost region		polygons
Soil class, soil properties, C density	Mishra et al. (2021)		Machine learning using harmonized soil profiles and remote-sensing data products	Permafrost region	250 m	Raster
Soil class, soil properties, C density	Hengl et al. (2017); Poggio et al. (2021)	SoilGrids250 m/ 2.0	Machine learning using soil profiles and remote-sensing data products	Global	250 m	Raster

characteristics of permafrost under relatively stable conditions can be adequately quantified (i.e., static maps), dynamically mapping these under rapidly changing climate conditions remains a challenge, hindering our understanding of the large-scale extent and implications of permafrost thaw.

## 1.2. Permafrost Region Vegetation: A Key Control on C Cycling

There is considerable variation in northern permafrost region vegetation from the sparsely vegetated low-statured treeless tundra environments to the densely vegetated boreal forests in the south. High densities of lakes, ponds, and wetlands are found in these northern high latitudes, with wetlands alone covering between 5% and 25% of the permafrost region (Figure 1; Karesdotter et al., 2021; Olefeldt et al., 2021; Raynolds et al., 2019). Extensive lake and peatland formation is linked to the relatively flat landscapes created by glacial retreat, increases in available moisture, and thermokarst development (Alexandrov et al., 2016; Brosius et al., 2021; Gorham et al., 2007). Tundra vegetation is often distributed along soil moisture gradients, with graminoid vegetation found in areas with high soil moisture (e.g., topographical depressions or flat areas), whereas shrubs dominate in better drained, more elevated or sloping areas (Heijmans et al., 2022). Evergreen forests comprise the majority of boreal forests in the North American permafrost region followed by deciduous broadleaf forests (Wang et al., 2020); deciduous larch forests cover large areas in the Russian permafrost region (Shevtsova et al., 2020).

Warming in the permafrost region is expected to enhance vegetation growth as well as shift species composition, which can affect C cycling both directly and indirectly. Vegetation changes have consequences for many additional ecosystem functions through effects on energy balance, hydrology, soil temperatures, C inputs to soil, and susceptibility to wildfire (Chapin et al., 1996; Mack et al., 2021; Sturm et al., 2005). Both greening (enhanced vegetation productivity; often associated with tree and shrub expansion) and browning (decreased productivity due to vegetation dieback or slower growth) are expected in permafrost regions under current warming trajectories, although the responses differ locally (Berner et al., 2020; C. X. Liu et al., 2021; Myers-Smith et al., 2020; Reid et al., 2022). Greening during the 1985–2016 has been more widespread, covering ca. 37% of the tundra, whereas browning occurs in only 5% of the tundra (Berner et al., 2020). Meta-analyses of direct warming effects on vegetation suggest that warming increases vascular plant abundance and height, especially shrubs, but again, results are spatially variable (Elmendorf et al., 2012; Sistla et al., 2013). Permafrost thaw can also increase nutrient availability and contribute to increased productivity (Hewitt et al., 2019; Salmon et al., 2016). However, enhanced vegetation growth may not translate into enhanced ecosystem C stocks due to feedbacks between snow conditions and soil temperatures, vegetation, litter, and decomposition (Hartley et al., 2012; Sistla et al., 2013). For example, increased plant growth (both above- and belowground) could increase C inputs to soil, but enhanced root-derived C into soils could also increase soil C decomposition via microbial priming (Keuper et al., 2020). Recent reviews discuss interactions between shrub expansion (shrubification), permafrost, and C cycling with the overall conclusion that it is not known whether shrubification results in increased or decreased soil carbon stocks (Heijmans et al., 2022; Mekonnen et al., 2021).

Many spatial data products are available to map ecosystem types in the permafrost region based on vegetation or land cover. These map products, ranging from global to regional coverage, are often used for spatial extrapolation of processes related to permafrost C cycling including soil mapping (Mishra et al., 2021; Palmtag et al., 2022) and for upscaling C fluxes (Virkkala et al., 2021a). The most widely-used vegetation map, the Circumpolar Arctic Vegetation Map, is pan-Arctic in extent but does not include the boreal or sub-Arctic parts of the permafrost region (Raynolds et al., 2019; D. A. Walker et al., 2005). Global products often fail to separate key land cover types for permafrost C cycling, such as different dominant tree species, shrub and wetland types (Chasmer et al., 2020). As image resolution improves, higher resolution vegetation classifications can be expected but will require additional approaches to overcome limitations in determining critical land cover types.

## 1.3. Permafrost Soils: A Globally Significant C Reservoir

Soils within the permafrost region have accumulated C over millennia, with different dynamics depending on the extent of glaciation during the last glacial maximum (LGM; Harden et al., 1992; Lindgren et al., 2018). Northern peatlands and soils are distributed across the permafrost region in areas that were glaciated at LGM (Figure 1a) and contain substantial C stocks (Frolking et al., 2011; Yu et al., 2010). Large C stocks in areas that were not glaciated at LGM (Figure 1a), such as the Yedoma region, generally accumulated during the Pleistocene and consist of perennially frozen, fine-grained, organic-bearing, and ice-rich sediments (Strauss et al., 2017). The accumulation and persistence of soil C in this region are driven by limitations on decomposition of soil organic matter by temperature and soil saturation as well as repeated frost heave (cryoturbation) or repeated sediment deposition, which incorporates soil C from the surface deeper in the soil profile (Harden et al., 2012; Strauss et al., 2017). These processes have resulted in large soil C stocks within the permafrost region, with best estimates

ranging from 1,014 (95% CI: 839–1,208) to  $1,035 \pm 150$  Pg C for 0–3 m depth (Hugelius et al., 2014; Mishra et al., 2021) and 1,307 Pg C including deep (>3 m depth) Yedoma deposits, deltaic alluvium, and peats (Strauss et al., 2021). The most carbon-rich reservoirs in the 0–3 m of the permafrost soils are in peatlands and some tundra regions primarily in Hudson Bay Lowland, West Siberian Lowlands, western parts of the Northwest Territories, Alberta and British Columbia in Canada, and parts of northern Alaska (Figure 1b; Hugelius et al., 2014; Tarnocai et al., 2009).

Deep soil C deposits have been the most challenging reservoirs to quantify, but new estimates have recently been published for peatlands and Yedoma deposits (Figure 1a; Hugelius et al., 2020; Strauss et al., 2021; Strauss et al., 2017). These estimates highlight the critical role of peat deposits in the overall C stock of the permafrost region, including areas with and without permafrost (Hugelius et al., 2020). The insulating properties of peat can protect permafrost from thawing, resulting in the presence of residual or relict patches of permafrost in landscapes otherwise free of permafrost (Shur & Jorgenson, 2007; Vitt et al., 2000). Northern peatlands store approximately  $415 \pm 147$  Pg C in peat, of which  $185 \pm 66$  Pg C is located in permafrost-affected peatlands (Hugelius et al., 2020); a synthesis dataset of permafrost peat properties showed that permafrost formation in peatlands can both enhance or decrease C accumulation rates depending on site characteristics and timing of formation (Treat et al., 2016).

Yedoma deposits can reach a thickness of up to tens of meters and often containing large syngenetic ice wedges. Today, these are found in areas that remained deglaciated during the last glaciation of Siberia, Alaska and the Yukon (Figure 1a), and contain 115 Pg C (95% CI: 83–129 Pg C; Strauss et al., 2021). Together with other deep deposits in the Yedoma domain such as Holocene thawed and refrozen sediment, the Yedoma domain contains 400 Pg C (95% CI: 327–466 Pg C; Strauss et al., 2017). Arctic delta deposits are also considered as deep (up to 60 m depth), heterogeneous deposits (H. J. Walker, 1998) and are estimated to store approximately 67 Pg organic carbon but this estimate is highly uncertain (Hugelius et al., 2014). Due to increasing river discharge, sea level rise and permafrost thaw, Arctic delta sediment deposits might degrade and thaw resulting in a release of bio-available C into the near-shore of the Arctic Ocean or as CO<sub>2</sub> into the atmosphere (Overeem et al., 2022).

The most recent terrestrial C stock estimates for the permafrost region have incorporated over 2,700 soil profiles, but northern regions are still under-sampled compared with temperate regions (Mishra et al., 2021). Overall, permafrost region C stock estimates have been improved by concerted efforts to compile, harmonize, synthesize, and create open datasets of existing soil profile characterizations (Malhotra et al., 2019; Palmtag et al., 2022; Tarnocai et al., 2009). Hugelius et al. (2014) discuss remaining sources of uncertainty in the soil C dataset for the permafrost region, which include extensive spatial gaps over Russia, Scandinavia, Greenland, Svalbard and eastern Canada. Areas with thin soils and low C stocks in the High Arctic and mountainous regions also remain under-sampled, contributing to high uncertainty in spatially explicit C density mapping (Mishra et al., 2021). Other key data gaps include Arctic delta deposits and peat deposits buried under mineral soils that glaciation and permafrost have preserved (Treat et al., 2019). Understanding how soil C stocks will change with disturbance continues to be an important topic, including the response to gradual and abrupt permafrost thaw and resulting hydrologic changes (e.g., M. C. Jones et al., 2017; Plaza et al., 2019).

## 2. Terrestrial Carbon Fluxes in the Permafrost Region

### 2.1. CO<sub>2</sub> and CH<sub>4</sub> Flux Magnitudes and Underlying Mechanisms

Northern permafrost regions have been a net sink of atmospheric CO<sub>2</sub> and smaller source of CH<sub>4</sub> since the beginning of the Holocene (Frolking & Roulet, 2007; Harden et al., 1992; Lindgren et al., 2018; Shi et al., 2020). Overall, carbon uptake has exceeded carbon emissions, as evidenced by the large soil carbon stocks of the region. For recent decades (primarily 1990–2015), estimates of mean annual terrestrial net ecosystem exchange (NEE, i.e., the balance between gross primary productivity (GPP) and ecosystem respiration, ER) range from  $-1,800$  (net sink) to 600 Tg C yr<sup>-1</sup> (net source) (Bruhwiler et al., 2021; McGuire et al., 2016; Virkkala et al., 2021a; Watts et al., 2023), with most of the recent estimates averaging at  $-300$  Tg C yr<sup>-1</sup> (Watts et al., 2023). Wetlands and lakes in the permafrost region emit between 5.3 and 37.5 Tg CH<sub>4</sub>-C yr<sup>-1</sup> (net source), with the majority of estimates being close to 22.5 Tg CH<sub>4</sub>-C yr<sup>-1</sup> (Bruhwiler et al., 2021; Christensen et al., 2017; McGuire et al., 2012; McNicol et al., 2023; Peltola et al., 2019a). However, the spatial domains included in these reviews were variable and were sometimes based on latitudinal limits (e.g.  $>60^\circ$  N) or the entire Arctic-boreal or permafrost regions. In addition to ecosystem-mediated C exchange, direct emissions from Arctic-boreal fires are between 100 and

400 Tg C yr<sup>-1</sup> (on average 142 Tg C yr<sup>-1</sup>) (McGuire et al., 2016; van Wees et al., 2022; Veraverbeke et al., 2021). Lateral fluxes of CO<sub>2</sub>, CH<sub>4</sub>, and dissolved organic matter from terrestrial ecosystems to riverine and lacustrine systems can comprise a key part of the C budgets, ranging from 2% to 16% of NEE in areas with intact permafrost or up to 60% of NEE in upland areas experiencing thaw slumping (McGuire et al., 2009; Olefeldt et al., 2012; Zolkos et al., 2022). Earlier reviews have discussed lateral fluxes and controls on aquatic system C cycling in the permafrost region (Ramage et al., 2023; Tank et al., 2020; Vonk et al., 2015). Here, we focus on terrestrial ecosystem C exchange with the atmosphere.

The annual CO<sub>2</sub> sink is primarily driven by intense plant activity during the relatively short growing seasons (typically lasting 2–5 months; Lund et al., 2010; Virkkala et al., 2021a). However, the net ecosystem C accumulation is driven by belowground dynamics in soils and biomass rather than accumulation in above-ground vegetation C stocks (Bradshaw & Warkentin, 2015; Hartley et al., 2012; Shaver et al., 1992). The growing season sink strength has been relatively well synthesized across different moisture gradients and continents (McGuire et al., 2012), biomes (Virkkala et al., 2021), and vegetation types (Ramage et al., 2023). Net growing season C uptake is highest in the boreal permafrost region, particularly in warm evergreen and larch forests and can range between  $-150$  and  $-240$  g C m<sup>-2</sup> month<sup>-1</sup> during the June–August period (Hiyama et al., 2021); moist to wet graminoid-dominated tundra ecosystems also show strong growing season C uptake between  $-90$  and  $-150$  g C m<sup>-2</sup> month<sup>-1</sup> (Celis et al., 2017; Kittler et al., 2017; Pirk et al., 2017). Peatlands have low rates of net CO<sub>2</sub> uptake both from low plant productivity and even lower rates of decomposition due to anoxic soil conditions (Euskirchen et al., 2014; Frolking et al., 2011); mean long-term apparent C accumulation rates range from 20 to 35 g C m<sup>-2</sup> y<sup>-1</sup>, but are higher in recently accumulated peat and lower in boreal permafrost peatlands (14 g C m<sup>-2</sup> y<sup>-1</sup>; Treat et al., 2016).

Arctic and permafrost regions are a net source of CH<sub>4</sub> to the atmosphere (McGuire et al., 2012; Saunois et al., 2020). Methane emissions are the net of production in anoxic soils and oxidation in the overlying aerobic soils, which can be bypassed by plant-mediated transport and ebullition (Christensen et al., 2003; Whalen, 2005). Methane fluxes from permafrost regions can show different patterns than permafrost-free regions. Unlike upland areas in temperate regions that are net sinks of atmospheric CH<sub>4</sub> (Le Mer & Roger, 2001), upland (i.e., non-wetland) areas in tundra and boreal forest can be net CH<sub>4</sub> sources to the atmosphere due to periodically saturated conditions and cold-season emissions (Hashemi et al., 2021; Hiyama et al., 2021; Kuhn et al., 2021b; Treat et al., 2018b; Zona et al., 2016). However, upland tundra can also oxidize more CH<sub>4</sub> than previously thought (Jorgensen et al., 2015; Oh et al., 2020; Voigt et al., 2023); understanding the controls on these differences and net effect remains to be explored. For permafrost wetlands, CH<sub>4</sub> emissions are generally smaller than in permafrost-free wetlands due to the lower temperatures (Kuhn et al., 2021b; Olefeldt et al., 2013; Treat et al., 2018b). Moreover, airborne data have helped detect unexpectedly high CH<sub>4</sub> emissions from tundra (Miller et al., 2016), hotspots at lake margins (Elder et al., 2021), and strong geologic emissions in the Mackenzie River Delta (Kohnert et al., 2017). Some emissions hotspots are known to be thermogenic CH<sub>4</sub> (Kleber et al., 2023; Kohnert et al., 2017; Walter Anthony et al., 2012). Several previous efforts have extensively reviewed aspects of CH<sub>4</sub> fluxes in northern regions including key abiotic drivers such as temperature, water table position, and vegetation (Bridgman et al., 2013; Kuhn et al., 2021b; Olefeldt et al., 2013; Segers, 1998; Whalen, 2005), interactions with vegetation (Bastviken et al., 2022), feedbacks to climate (Dean et al., 2018), in peatlands (Blodau, 2002; Lai, 2009), production rates (Schädel et al., 2016; Treat et al., 2015), and generally for the permafrost region (Miner et al., 2022).

*In-situ* terrestrial CO<sub>2</sub> and CH<sub>4</sub> fluxes in the permafrost region have been synthesized in nearly 20 studies over the past decades with varying spatial extents (Figure 2). Virkkala et al. (2022) summarized the existing CO<sub>2</sub> flux syntheses for the permafrost region (Table 1 in Virkkala et al., 2022; Figure 2b here), showing an increase in CO<sub>2</sub> flux measurements over time in the permafrost region from  $\sim 30$  sites to over 200 sites in just one and a half decades. However, these 200 sites are not all currently active; the number of active eddy covariance sites measuring CO<sub>2</sub> and CH<sub>4</sub> fluxes in 2022 was 119 and 45 sites, respectively (Pallandt et al., 2022). Methane fluxes have been synthesized in 10 studies for both the permafrost region as well as smaller regions (Figure 2, Table 2); recent syntheses include between 18 (eddy covariance) and 96 (eddy covariance + flux chambers) unique sites in the permafrost region.

A key motivation for these syntheses has been to quantify CO<sub>2</sub> and CH<sub>4</sub> flux magnitudes and their controls across the permafrost region. Early estimates established that Arctic and boreal regions are a significant source of CH<sub>4</sub> to

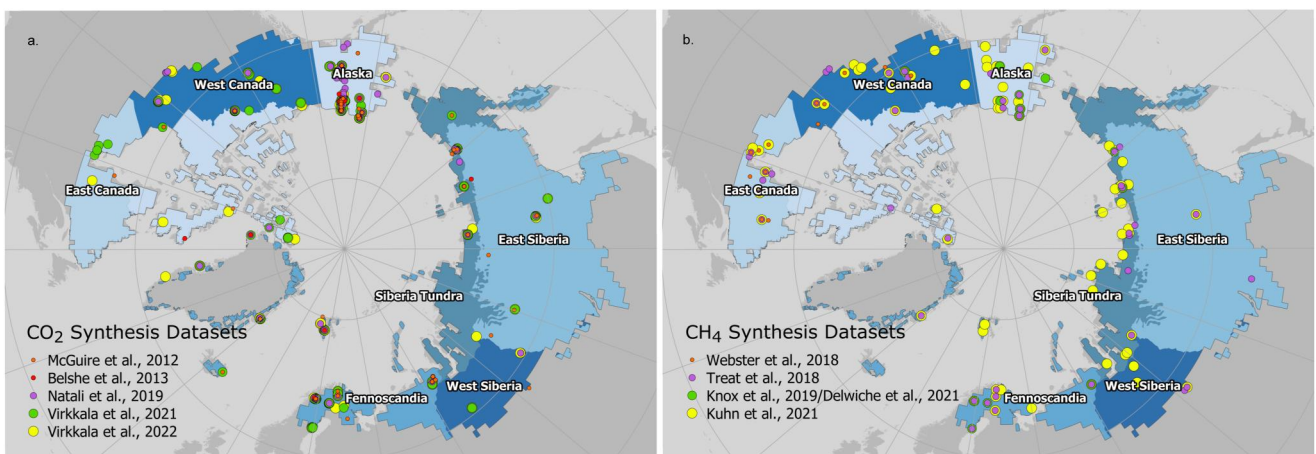


**Figure 2.** Maps showing the distribution of measurement sites included in existing synthesis products for both (a) CO<sub>2</sub> flux data syntheses (adapted from Virkkala et al., 2022; and (b) CH<sub>4</sub> flux data syntheses including both eddy covariance (FLUXNet; Delwiche et al., 2021; Knox et al., 2019), as well as eddy covariance and chambers covering both growing season, and annual emissions (Kuhn et al., 2021a; Treat et al., 2018a; Webster et al., 2018). The regions used in the analysis are labeled indicated in different shades of blue.

the atmosphere (Bartlett & Harriss, 1993; Matthews & Fung, 1987) but the CO<sub>2</sub> balance in the region has remained less certain (Chapin et al., 2000; Hayes et al., 2022). Recent *in-situ* estimates indicate that the boreal biome within the permafrost region has acted as an annual CO<sub>2</sub> sink over the past two decades, while the tundra biome appears to be either CO<sub>2</sub> neutral or a small CO<sub>2</sub> source, although there is considerable uncertainty associated with these findings (Bradshaw & Warkentin, 2015; Z.-L. Li et al., 2021; Natali et al., 2019; Virkkala et al., 2021a). Some parts of the permafrost region, such as Alaska, might be annual net CO<sub>2</sub> sources in both biomes (Commane et al., 2017).

The existing CH<sub>4</sub> flux syntheses have established the magnitude of CH<sub>4</sub> fluxes during the growing season and annual emissions for a wide range of sites and ecosystems across the northern permafrost region (Figure 2; Table 2). Multiple syntheses show significant differences in CH<sub>4</sub> emissions observed among wetland classes and compared to uplands (Figure 3; Knox et al., 2019; Kuhn et al., 2021b; Treat et al., 2018b). Specifically, marshes and fens have significantly larger CH<sub>4</sub> fluxes than permafrost bogs (including palsas, peat plateaus) and upland tundra, ranging from 5.5x–7.5x larger to 18x–23x larger, respectively, as demonstrated by our quantitative summary of these syntheses shown in Figure 3. However, CH<sub>4</sub> fluxes from other permafrost wetlands do not differ significantly from the other wetland categories (marshes, fens, bogs), and differences between permafrost and non-permafrost bogs were not significant, implying that it is important to capture both permafrost (temperature/substrate) effects on CH<sub>4</sub> fluxes and vegetation differences, likely related to the presence of aerophytic plants facilitating CH<sub>4</sub> transport versus *Sphagnum* mosses and shrubs (Bastviken et al., 2022).

Emerging evidence highlights the key role of non-growing seasons in understanding the annual CO<sub>2</sub> and CH<sub>4</sub> balances (Commane et al., 2017; Natali et al., 2019; Treat et al., 2018b; Zona et al., 2016). Shoulder seasons, the transition periods close to the growing season (i.e., spring and fall), may be particularly important. For example, in fall and early winter, deeper soils are often thawed despite soils at the surface being frozen, boosting decomposition of deeper (and potentially older) soil organic matter while plant activity remains limited (Euskerchen et al., 2017; Pedron et al., 2022; Schuur et al., 2009); increased connectivity with groundwater pathways may enhance export (Hirst et al., 2023). As the soils freeze and thaw during the “zero-curtain” window (Outcalt et al., 1990), microbial activity can persist at low rates even when average soil temperatures are at or below zero (Cleland & Schimel, 1995; Öquist et al., 2009). Emissions occurring during this extended period can add up to a substantial annual flux, up to 50% of annual ER and CH<sub>4</sub> emissions (Celis et al., 2017; Hashemi et al., 2021; Treat et al., 2018b; Zona et al., 2016). At some sites, the non-growing season CO<sub>2</sub> emissions currently offset or exceed growing season uptake and ultimately determine the annual C balance (Hashemi et al., 2021; Z. Liu et al., 2022; Watts et al., 2021). However, only ca. 20% of current eddy covariance sites measuring both CO<sub>2</sub> and CH<sub>4</sub> fluxes year-round; these sites are representative for only 10%–20% of the pan-Arctic (Pallandt et al., 2022). Most of these sites are in warmer areas that are in general easier to access and maintain (northern Scandinavia, Alaska,

**Table 2**  
Review of Existing Data Syntheses of  $CH_4$  Flux Measurements That Include the Northern Permafrost Region

Study	No. unique sites total/permafrost region <sup>a</sup>	Synthesized fluxes and measurement techniques ecosystem domain	Study domain	Study period	Flux aggregation	Format	Notes
Bartlett and Harriss (1993)	218 <sup>b/57<sup>c</sup></sup>	Chamber and eddy covariance	Global	Measurements from 1982 to 1991	Daily, Annual	Point-based	Dataset in Table
Nilsson et al. (2001)	619 <sup>b/-</sup>	Survey of chamber fluxes from across different wetlands in Sweden	Sweden	1994	Daily	Lacks spatial information	Reports characteristics fluxes of different wetland types
Frolking et al. (2011)	38 <sup>b/11</sup>	Chamber and eddy covariance	Global	Measurements from 1990 to 2008	Annual	Point-based	Mean annual $CH_4$ fluxes for northern peatlands and references included; dataset not included
McGuire et al. (2012)	63 <sup>b/63</sup>	Chamber, eddy covariance, diffusion-based concentration gradient estimates	Arctic	Measurements from 1974 to 2011	Daily, Seasonal, Annual	Point-based	Dataset in Appendix
Olefeldt et al. (2013)	303 <sup>b/-</sup>	Chamber	Permafrost region	Measurements from 1984 to 2010	Daily	Point-based	Dataset not publicly available but included in Kuhn et al. (2021)
Turetsky et al. (2014)	71 <sup>b/33<sup>d</sup></sup>	Chamber and eddy covariance	Global	Measurements from 1980 to 2011	Daily	Point-Based	Dataset not publicly available
Webster et al. (2018)	49/23	Chamber and eddy covariance	Canada	Measurements from 1984 to 2016	Daily, Seasonal, Annual	Point-based	Dataset not publicly available
Treat et al. (2018b)	173/62	Chamber, eddy covariance, & snowpack diffusion method	northern extra-tropical	1974–2016	Daily, Seasonal, annual	Point-based	Inclusion criteria: minimum 1 msmt/month during growing season
Delwiche et al. (2021); Knox et al. (2019)	81/17	Eddy covariance	Global	Measurements from 2006 to 2018	Half-hourly, Daily	Point-based	Data download only available for individual FluxNET sites, not as dataset
Kuhn et al. (2021b)	151 <sup>e/96</sup>	Chamber, eddy covariance, concentration gradient	northern permafrost region	Measurements from 1984 to 2019	Daily	Point-based/ Shapefile/ KML	Builds on Wik et al. (2016) and Olefeldt et al. (2013)

<sup>a</sup>Permafrost region defined as in this paper by RECCAP2 regions. <sup>b</sup>Could not assess whether included sites were unique, site numbers could include multiple plots or multiple year replicates. <sup>c</sup>Number from Arctic wetlands rather than RECCAP2 region and could include site duplicates. <sup>d</sup>Includes sites from sub-Arctic and boreal regions. <sup>e</sup>site analysis limited to terrestrial wetlands and uplands, excluding lakes and ponds.

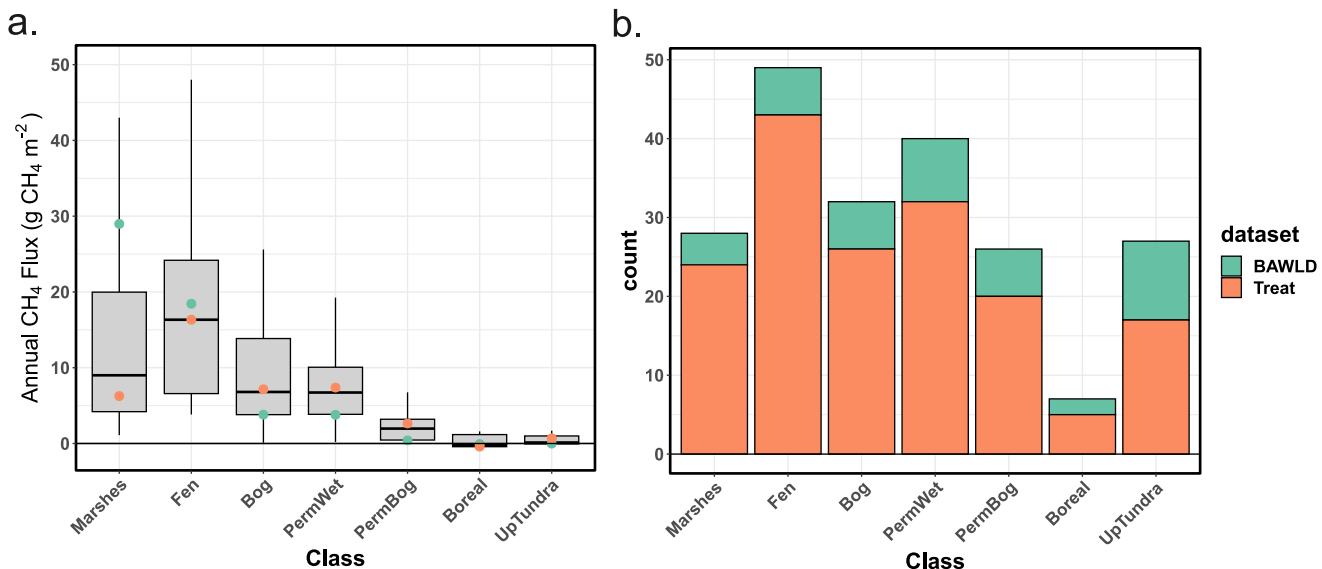


**Figure 3.** Annual CH<sub>4</sub> emissions (a) and number of measurements (b) for different ecosystem and wetland classes found in the permafrost region using two different synthesis datasets (BAWLD: Kuhn et al., 2021a; Treat et al., 2018a). Significant differences were found in CH<sub>4</sub> emissions between ecosystem classes ( $F_{6,202} = 6.0$ ,  $p < 0.0001$ ) but not between datasets. Ecosystem classes were categorized as marsh, fen, bog, permafrost wetland (PermWet), permafrost bog (PermBog, including peat plateaus and palsas), boreal forest (Boreal), and upland tundra (UpTundra).

southern parts of Canada), while areas that are more remote remain under sampled. Continued research on the evolving seasonal freeze-thaw and soil moisture dynamics and effects on C emissions following permafrost thaw is critical for gaining a deeper understanding of the permafrost C feedback.

## 2.2. Regional Variability in CO<sub>2</sub> and CH<sub>4</sub> fluxes

In addition to regional differences in climate warming, differences across the permafrost region may affect the vulnerability of permafrost C to decomposition and release to the atmosphere (Gulev et al., 2021; Jorgenson & Osterkamp, 2005). The permafrost region varies in characteristics such as temperature, permafrost extent, ice content, and the degree of ecosystem protection of permafrost (e.g., insulating organic layers) (e.g., Shur & Jorgenson, 2007). Together with variability in observed and projected degree of warming, this makes some areas more likely to experience widespread permafrost degradation than others (Fewster et al., 2022; Olefeldt et al., 2016). The abundance of lakes and wetlands, vegetation composition, permafrost growth and formation history, soil C stocks and geomorphology also differ across the permafrost domain (e.g., Sections 1.2, 1.3), influencing the controls on CO<sub>2</sub> and CH<sub>4</sub> fluxes over broad spatial scales.

As the number and distribution of measurement sites across the permafrost domain has grown, we can compare the different datasets and approaches across policy-relevant domains (Figure 2) to see how flux magnitude and direction differ (Supporting Information S1). We analyze regional variability of CO<sub>2</sub> and CH<sub>4</sub> fluxes using recently published datasets and models to study the general spatial patterns in C fluxes and convergence across datasets and models. Terrestrial ecosystem NEE fluxes are derived from various recent model inter-comparisons and outputs and *in-situ* synthesis datasets (Table S1 in Supporting Information S1); annual CH<sub>4</sub> fluxes are from two *in-situ* syntheses (Kuhn et al., 2021b; Treat et al., 2018b) and one statistical upscaling-based on eddy-covariance (Peltola et al., 2019a). For North America, the regions included Alaska, Canadian tundra, boreal Western Canada, and Eastern Canada. For Eurasia, these included Western Eurasia, Siberian tundra, Eastern Siberia, and Western Siberia. This regional approach can help to target new areas for measurements based on key differences indicative of a lack of understanding of the underlying processes. We limited these datasets to the permafrost region within the northern tundra and boreal biomes, similar to the Regional Carbon Cycle Assessment and Processes Project 2 (RECAP-2) permafrost effort (Ciais et al., 2022; Hugelius et al., 2023).

The results from our comparison among datasets and models show stronger regional CO<sub>2</sub> sinks in the southern permafrost region, while lower net CO<sub>2</sub> uptake or net CO<sub>2</sub> emissions occur toward the north (Figures 4 and 5).

**Table 3**

Mean and Standard Deviation of Annual Terrestrial NEE ( $\text{g C m}^{-2} \text{ yr}^{-1}$ ) for Key In-Situ and Model Ensemble Categories During 2002–2014 (for ISIMIP Process Models 2002–2005)

Model type	Alaska	Canadian tundra	Western Canada	Eastern Canada	Western Eurasia	Siberian tundra	Eastern Siberia	Western Siberia
<b>In-situ</b>	6 ( $\pm 52$ )(14 sites)	-22 (NA)(2 sites; non-growing season not directly measured)	-53 ( $\pm 84$ )(9 sites)	-40 ( $\pm 16$ )(3 sites)	-33 ( $\pm 51$ )(11 sites)	4 ( $\pm 27$ )(2 sites)	-64 ( $\pm 85$ )(3 sites)	NA
<b>Upscaling</b>	-6 ( $\pm 27$ )	13 ( $\pm 19$ )	-12 ( $\pm 27$ )	-38 ( $\pm 35$ )	-44 ( $\pm 45$ )	-3 ( $\pm 29$ )	-17 ( $\pm 27$ )	-6 ( $\pm 26$ )
<b>Inversion</b>	-3 ( $\pm 66$ )	-10 ( $\pm 30$ )	-74 ( $\pm 86$ )	-40 ( $\pm 79$ )	-27 ( $\pm 88$ )	-10 ( $\pm 72$ )	-47 ( $\pm 81$ )	-74 ( $\pm 86$ )
<b>CMIP6 process model</b>	-13 ( $\pm 32$ )	-5 ( $\pm 20$ )	-25 ( $\pm 43$ )	-30 ( $\pm 40$ )	-21 ( $\pm 37$ )	-5 ( $\pm 26$ )	-18 ( $\pm 19$ )	-27 ( $\pm 40$ )
<b>ISIMIP process model</b>	-39 ( $\pm 104$ )	-9 ( $\pm 24$ )	-52 ( $\pm 82$ )	-44 ( $\pm 43$ )	-56 ( $\pm 55$ )	-17 ( $\pm 34$ )	-33 ( $\pm 17$ )	-54 ( $\pm 50$ )

Note. The *in-situ* column also includes the number of sites from the entire permafrost domain which is relatively similar to the proportion of measurement years in total in the dataset. Standard deviations were calculated for each year and model separately and averaged across all models, and thus represents average standard deviation around the mean and describes the spatial flux variability within the region. Note that inversion estimates include lake  $\text{CO}_2$  fluxes as well, but fossil fuel emissions, cement carbonation sink, lateral fluxes and fire emissions have been masked away.

This regional pattern in  $\text{CO}_2$  fluxes is likely related to temperature, radiation regime, and growing season length, in agreement with earlier syntheses (McGuire et al., 2012; Virkkala et al., 2021a). The highest median annual  $\text{CO}_2$  sinks were located in western Canada ( $-52 \text{ g C m}^{-2} \text{ yr}^{-1}$ ) and western Siberia ( $-41 \text{ g C m}^{-2} \text{ yr}^{-1}$ ), and smallest  $\text{CO}_2$  sinks in Alaska ( $-6 \text{ g C m}^{-2} \text{ yr}^{-1}$ ) and Siberian tundra ( $-5 \text{ g C m}^{-2} \text{ yr}^{-1}$ ; Table 3). Some statistically significant differences occurred between regions that were strong sinks and small sinks to net sources (Figure 4;  $F_{7,31} = 4.29, p < 0.01$ ). The  $\text{CH}_4$  syntheses show highest annual fluxes from the Siberian tundra and Western Eurasian regions (Figure 5, median =  $15.5\text{--}17.9 \text{ g CH}_4 \text{ m}^{-2} \text{ yr}^{-1}$ ) but no statistically significant differences between regions were found.

Regional differences in wetland  $\text{CH}_4$  fluxes were highly variable among chamber-based synthesis studies (Figure 5a), with regional medians ranging from  $1.6$  to  $18 \text{ g CH}_4 \text{ m}^{-2} \text{ yr}^{-1}$ . The variability was smaller for the eddy-covariance based upscaling ( $5.7\text{--}13 \text{ g CH}_4 \text{ m}^{-2} \text{ yr}^{-1}$ ). Colder regions with thinner sediments in Canadian tundra and Eastern Canada tended to have lower  $\text{CH}_4$  fluxes (Figures 5a and 1a) while highest annual  $\text{CH}_4$  fluxes were found in Eurasia. Relatively few annual measurements have been reported for Hudson Bay Lowlands and Taiga Plains (Canada) and Western Siberia (Figures 2b and 5b), home to the largest peatland complexes in the world (Hugelius et al., 2020). Comparing the coefficient of variation among the datasets showed a mean of 0.29 across the regions with the best agreement in western Canada (0.05) and worst in eastern Canada (0.53), despite having a similar number of observations. Given that  $\text{CH}_4$  emissions vary strongly among wetland classes (Figure 3a), some variability among the methods may be due to differences among the wetland types measured and synthesized within the regions (Treat et al., 2018b), which may or may not reflect the distribution of wetland types across the landscape (Kuhn et al., 2021b; Olefeldt et al., 2021).

These synthesis datasets also show some biases toward C hotspots: most sites measuring  $\text{CO}_2$  and  $\text{CH}_4$  fluxes are in wetlands or moist-wet ecosystems with high  $\text{CH}_4$  emissions and high growing season  $\text{CO}_2$  sinks (Figure 3b; Virkkala et al., 2022). Drier ecosystems including boreal forests, sparsely vegetated regions, and mountainous areas remain less studied (Figure 3b; Pallandt et al., 2022; Virkkala et al., 2022) despite covering ca. 80% of the permafrost region (Karesdotter et al., 2021; Olefeldt et al., 2021). This limits our ability to detect changes in C fluxes because even small changes in the site distribution (e.g., new sites being set up in new environments), methodology (e.g., chambers or towers synthesized), and data coverage can impact the average sign of fluxes or direction in trends when data are aggregated over larger domains (Belshe et al., 2013; McGuire et al., 2012).

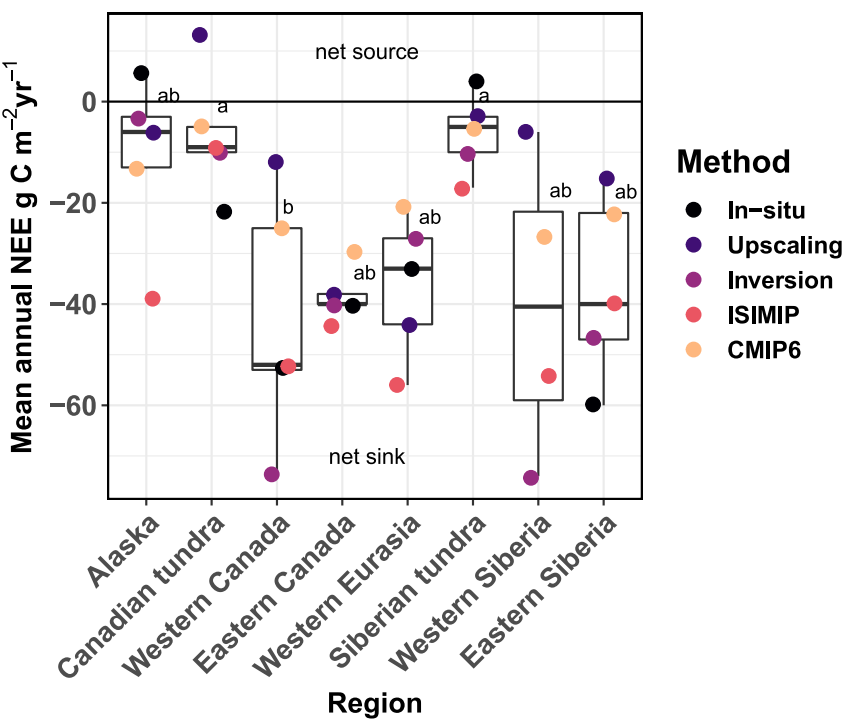


**Figure 4.** A comparison of regional terrestrial annual NEE over 2002–2014 across the main model and synthesis categories. Regional differences in NEE were statistically significant ( $p = 0.0014$ ). Each region that shares a mean not statistically different ( $p > 0.05$ ) from another one based on Tukey's test shares the same letter.

Manual flux chamber measurements are distributed more broadly across the permafrost region than eddy covariance measurements and could help to offset some spatial biases and data gaps, particularly for  $\text{CH}_4$  fluxes (Figure 2). However, barriers remain to using these manual chamber data for modeling because of the limited spatial and temporal scales of measurements; statistical upscaling may offer some possibilities to further use these data (Natali et al., 2019; Virkkala et al., 2021a). Semi-permanent mobile towers or automated chambers could be utilized to enhance spatial coverage and complement the existing flux network of long-term monitoring sites (Varner et al., 2022; Voigt et al., 2023). Further improvements in flux estimates can be expected as new sites are

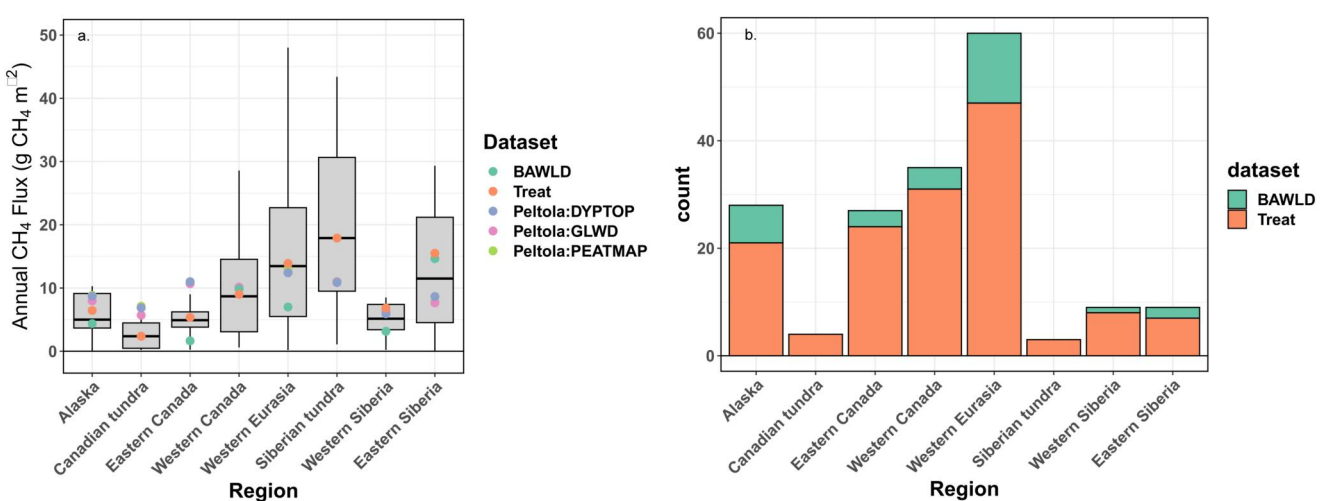


**Figure 5.** Annual areal  $\text{CH}_4$  emissions for wetlands (a) and number of measurements (b) among the study regions using different synthesis datasets (BAWLD: Kuhn et al., 2021a; Peltola et al., 2019a, 2019b; Treat et al., 2018a). Boxplots are derived from observations in BAWLD and Treat datasets; Peltola synthesis values are shown with values derived from the maps of different wetland distribution. No significant differences were found in  $\text{CH}_4$  emissions among regions.

added, more recent data are integrated to repositories, and newer methods are developed to leverage the sparse and disparate existing datasets.

### 2.3. Long-Term Trends in CO<sub>2</sub> and CH<sub>4</sub> Fluxes

How CO<sub>2</sub> and CH<sub>4</sub> exchange have changed over time in the permafrost region remains unknown. Circumpolar CO<sub>2</sub> trend analyses show an increasing growing season sink in the tundra (Belshe et al., 2013), a small and relatively negligible trend in non-growing season NEE in the permafrost region (Natali et al., 2019), but no clear changes in annual NEE despite increases in GPP and ER in the tundra (Belshe et al., 2013; Z.-L. Li et al., 2021). Long-term (>15-year) of measurements of CO<sub>2</sub> in sub-Arctic tundra sites show diverging trends: one shows an increasing net loss of CO<sub>2</sub> (Schuur et al., 2021), while the other shows enhanced CO<sub>2</sub> uptake following changes in vegetation with permafrost thaw (Varner et al., 2022).

Long-term measurements of CH<sub>4</sub> fluxes are rare (Christensen et al., 2017; Pallandt et al., 2022) but flux magnitudes have been shown to be increasing at the site-level for two permafrost sites in Eurasia over the past decades (Rößger et al., 2022; Varner et al., 2022). However, in North America, an analysis of concentration enhancements on the Alaska North Slope found no change in CH<sub>4</sub> flux magnitude over time (Sweeney et al., 2016). Similarly, there was no trend in 10 years of CH<sub>4</sub> flux measurement at a fen in interior Alaska (Olefeldt et al., 2017). Unfortunately, the data density in the CH<sub>4</sub> synthesis datasets included here was not sufficient to detect trends in emissions (e.g., Basu et al., 2022) or response to regionally warm and wet conditions that might enhance wetland CH<sub>4</sub> emissions to the extent that they affect global atmospheric CH<sub>4</sub> concentrations (Peng et al., 2022). Additional long-term measurements are needed to establish whether trends are occurring against a background of interannual variability and local processes (Hiyama et al., 2021). A synthesis of the limited long-term records of CO<sub>2</sub> and CH<sub>4</sub> exchange across multiple sites within the permafrost domain would be valuable.

### 2.4. CO<sub>2</sub> and CH<sub>4</sub> fluxes in Changing and Disturbed Environments

Understanding trends in C fluxes is challenging, because climate warming is affecting the timing and characteristics of seasonality in permafrost ecosystems, which has complex interactions with the environmental controls on C cycling. Warmer air temperatures in the winter and shoulder seasons result in longer duration of soil thaw (Farquharson et al., 2022; Y. Kim et al., 2012), lengthening the duration of microbial activity in the soil and affecting cold season fluxes as discussed above. The timing of snowmelt and the onset of the growing season are key controls of growing season NEE (Bellisario et al., 1998; Groendahl et al., 2007); the timing of these events has shifted earlier in the last decades (Xu et al., 2018). There is some evidence that the lengthening of the growing season increases the growing season C sink due to enhanced plant C uptake and increased vegetation biomass (Belshe et al., 2013; Bruhwiler et al., 2021). However, interactions with moisture seem to be a key determinant of the net growing season C uptake. For example, warmer peak growing season temperature can increase net summer C uptake through enhanced photosynthesis but warming also increases evapotranspiration, reducing available soil moisture and potentially increasing ER (J. Kim et al., 2021). Further, while earlier snowmelt might enhance net C uptake at the beginning of the growing season, the dry and warm conditions resulting from earlier snowmelt might increase ecosystem CO<sub>2</sub> losses during the late growing season (Belshe et al., 2013; Helbig et al., 2022). Further observations and enhanced linkages between biophysical processes, vegetation, and C cycles are needed.

Permafrost thaw and the associated carbon feedbacks have been increasingly well-studied (Schuur et al., 2022; Sjöberg et al., 2020; Virkkala et al., 2018), both as gradual thaw and abrupt thaw. Site-level studies indicate that CH<sub>4</sub> and CO<sub>2</sub> emissions can be strongly positively correlated with active layer depth due to the effects of increasing soil temperature on microbial activity, so gradual thaw of permafrost that deepens the soil active layer results in larger C emissions (Celis et al., 2017; Galera et al., 2023). Estimates of C loss from abrupt thaw may exceed those from active layer deepening but are highly uncertain (Estop-Aragonés et al., 2020; Zolkos et al., 2022). For example, less than ten site-level studies were available to use for a recent *in-situ*- based greenhouse gas budget estimate that showed that areas affected by abrupt thaw were net emitters of 31 (21, 42) Tg CO<sub>2</sub>-C yr<sup>-1</sup> and 31 (20, 42) Tg CH<sub>4</sub>-C yr<sup>-1</sup> (Ramage et al., 2023; Turetsky et al., 2020); the large uncertainties represent the potential spatial distribution of abrupt thaw areas that have only been quantified in limited regions (Nitze et al., 2018). To our knowledge, terrestrial sites experiencing abrupt thaw that have measured multi-year CO<sub>2</sub> or CH<sub>4</sub> fluxes are limited to wet graminoid ecosystems in Alaska (Schuur et al., 2021), boreal black spruce

lowlands in Canada and Alaska (Euskirchen et al., 2017; Helbig et al., 2017), and collapsing palsas from Fennoscandia (Varner et al., 2022). However, the current site network misses thaw slumps, gullies, and active layer detachments (Cassidy et al., 2016) that cover <1% of the areas affected by abrupt thaw; overall abrupt thaw is estimated to affect ~7% of the permafrost region in total (Ramage et al., 2023). Gradual and abrupt permafrost thaw cause changes in hydrology, often increasing soil moisture and/or lake extent, thus often increasing CH<sub>4</sub> emissions (Helbig et al., 2017; Miner et al., 2022; Varner et al., 2022). Many sites that have been observed to experience gradual or abrupt permafrost thaw are currently net C sources to the atmosphere (Euskirchen et al., 2017; Schuur et al., 2021); historically, some sites have shifted back to sequestering C centuries to millennia after permafrost thaw (M. C. Jones et al., 2017; Walter Anthony et al., 2014) but it is unclear whether this can be expected in the next centuries if temperatures continue to rise (M. C. Jones et al., 2023).

Warming is increasing the magnitude, extent, and severity of other disturbances in the permafrost region including wildfire, insect outbreaks, flooding, and drought (Foster et al., 2022; Meredith et al., 2019). These disturbances can impact C cycling directly through, for example, C emissions from fire combustion, and indirectly, by altering environmental conditions that control C fluxes, such as soil moisture, temperature, light availability, and species composition. Wildfire extent and severity has been increasing in the past decades (M. W. Jones et al., 2022); wildfire-induced changes to vegetation and soils can affect permafrost stability (Holloway et al., 2020), likely driving compounded effects on ecosystem C cycling (Harden et al., 2006; X.-Y. Li et al., 2021; Mack et al., 2021). The time required for C accumulation post-fire to offset wildfire C emissions takes decades and remains an open question (Mack et al., 2021; Ueyama et al., 2019; X. J. Walker et al., 2019). Additionally, overwintering fires are fundamentally changing fire dynamics and accelerating the fire season (Scholten et al., 2021). The effects of insect outbreaks might be severe during the outbreak but increased C uptake during the following years can compensate for the earlier losses (Lund et al., 2017; Ruess et al., 2021). Similar dynamics might occur with extreme meteorological events such as drought, flooding, and lack of snow but impacts are unclear (Olefeldt et al., 2017; Treharne et al., 2019). Interactions between permafrost, large herbivores, and soil C are an interesting area of research, however, the introduction of large herbivores is unlikely to stop the increasing carbon emissions from permafrost thaw at a circumpolar scale (Zimov et al., 2009). Increasing human presence is also impacting Arctic lands (Friedrich et al., 2022), but little is understood about effects on emissions such as increased fugitive CH<sub>4</sub> emissions (e.g., leaky infrastructure; Klotz et al., 2023), land use change emissions (Strack et al., 2019), or effects of the interactions between land use change and permafrost thaw (Ward Jones et al., 2022). Overall, an improved understanding requires new cross-disciplinary approaches to understand the magnitude of these processes across the entire permafrost domain.

### 3. Modeling the Carbon Fluxes in the Terrestrial Permafrost Region

#### 3.1. Main Modeling Approaches for C Exchange

Bottom-up C cycle models, that is, mechanistic process models, statistical and machine learning-based upscaling approaches, and top-down models (atmospheric inversions) are critical tools for estimating permafrost region C budgets. Process models are widely used to extrapolate and predict C fluxes both into the past and future (Koven et al., 2015; Lawrence et al., 2012; McGuire et al., 2016, 2018b) because they represent mechanistic understanding of processes at various scales. In the context of Arctic-boreal C budgets, land surface models (LSMs) of varying complexity can be used to represent relevant processes, such as dynamic vegetation and permafrost carbon. These can either be included within an earth system model (ESM) or driven in standalone mode by meteorological data. ESMs simulate coupled and dynamic interactions between Earth's climate system of oceans, atmosphere, cryosphere, and land surface and can include feedbacks from the land surface onto the atmosphere (Fisher et al., 2014). In addition to individual process-based models, coordinated research collaborations facilitating large model intercomparisons and ensembles (MIPs) have been key in exploring C budgets and several process model intercomparison studies exist for the permafrost region in addition to individual process models (McGuire et al., 2012, 2016, 2018b).

A few pan-Arctic studies have used statistical and machine learning models to upscale recent or current C fluxes at high spatial resolutions across larger domains or higher temporal resolutions (Jung et al., 2020; McNicol et al., 2023; Natali et al., 2019; Peltola et al., 2019a; Virkkala et al., 2021a). Earlier approaches often used simpler empirical upscaling of flux measurements (e.g., Bartlett & Harriss, 1993). These model types can be flexible with driver data and new datasets can thus easily be integrated but they have limited predictive capability; here, data

assimilation systems such as the CARbon DAta MOdel (CARDAMOM) that integrates various data sources with less complex process models might be a solution for better predictions (López-Blanco et al., 2019; Y. Q. Luo et al., 2012). Additionally, top-down atmospheric inversion models are constrained by atmospheric data where concentration changes are linked to flux and atmospheric transport and are often spatially coarser than the bottom-up approaches (Bruhwiler et al., 2021; Byrne et al., 2023; Z. Liu et al., 2022).

Bottom-up and top-down models have different main uses as well as strengths and limitations. Flux upscaling using statistical and machine learning approaches is still a relatively new field and has only been used in a few pan-Arctic studies; model intercomparisons may not yet be possible and may be limited by the number of pan-Arctic sites. Inversions have been used in permafrost region flux studies for over a decade already, but the number of inversion intercomparisons is still relatively low, and atmospheric observations in this area are scarce (Bruhwiler et al., 2021; Z. Liu et al., 2022; McGuire et al., 2012). In summary, bottom-up and top-down approaches complement each other and are important for predicting C emission and uptake patterns across the permafrost region.

### 3.2. Modeling Insights Into CO<sub>2</sub> Cycling in the Permafrost Region

Here we compared magnitudes of NEE among process-based modeling, inversion modeling, and statistical upscaling of *in-situ* data approaches for the regions used in earlier analysis (Supporting Information S1, Table 1). The models include results from the Coupled Model Intercomparison Phase 6 (CMIP6) assessed for the IPCC AR6 report (Canadell et al., 2021; IPCC, 2021), and the Inter-Sectoral Impact Model Intercomparison Project (ISIMIP), which provides historical runs and projections across the 21st century using various different driving data (Lange, 2019); other intercomparison projects not addressed here include the Coupled Climate Carbon Cycle MIP (C4MIP; Canadell et al., 2021), the TRENDY project (Friedlingstein et al., 2022; Sitch et al., 2015), and the Multi-scale Synthesis and Terrestrial Model Intercomparison Project (MsTMIP; Huntzinger et al., 2020).

In general, models and *in-situ* data had some agreement in regional NEE estimates with many of the approaches in each region agreeing on the sign of NEE (i.e., net sink or source). However, differences in NEE among approaches were still relatively high, with the average range of annual NEE estimates of 41 g C m<sup>-2</sup> yr<sup>-1</sup> (Figures 4 and 6). The best agreement in average NEE was found in the Siberian tundra and Eastern Canada which were small to moderate CO<sub>2</sub> sinks, respectively (Figure 4). This was unexpected, because these are also areas that have low flux data coverage (Table 3). The largest variability in mean NEE was found in western Siberia where the ISIMIP and inversion models showed a much stronger (>25 g C m<sup>-2</sup> yr<sup>-1</sup>) average sink than the other approaches; recent remote sensing analyses show a decreasing sink strength in Siberia driven by disturbance (Fan et al., 2023). While part of this disagreement is simply due to the high overall fluxes in this forest-dominated region, new measurements and process-level understanding of disturbance effects in this domain are critical to resolving this issue.

The largest differences among approaches were found between ISIMIP models and *in-situ* and/or upscaled estimates (e.g., in Alaska and Siberian tundra; Figures 4 and 6). This might suggest that the ISIMIP LSMs underestimate CO<sub>2</sub> emissions in this region, assuming that *in-situ* based estimates are reliable and representative of each region (Figure 4). The CMIP6 ESMs show weaker sink strength than both the ISIMIP LSMs and the inversions (both on average ca. 20 g C m<sup>-2</sup> yr<sup>-1</sup> weaker), which might be related to CMIP6 models underestimating the C sink strength in the permafrost region (see Section 3.3). While one could assume that the *in-situ* based averages and upscaling provide the most accurate estimates as they integrate recent data, they also suffer from severe data gaps and thus extrapolation uncertainties in some regions (see Section 2.2). Overall, the variability among approaches highlights the need for both additional data and development of predictive models as discussed in key challenges below.

### 3.3. Key Advancements and Challenges in Modeling Carbon Cycling in the Permafrost Region

LSMs have improved their representation of permafrost over the years, for example, by realistically simulating the thermal and hydraulic properties of soil, including phase change of soil water, and by accounting for the insulating effects of moss and snow cover (Chadburn et al., 2015; Ekici et al., 2014; Nicolsky et al., 2007). Despite these important advances to their land surface schemes, the CMIP6 ESMs included in the latest IPCC report still have a limited representation of C cycle processes in high-latitude regions. In the CMIP6 model ensemble, soil C stocks across the permafrost region were severely underestimated (Varney et al., 2022), likely

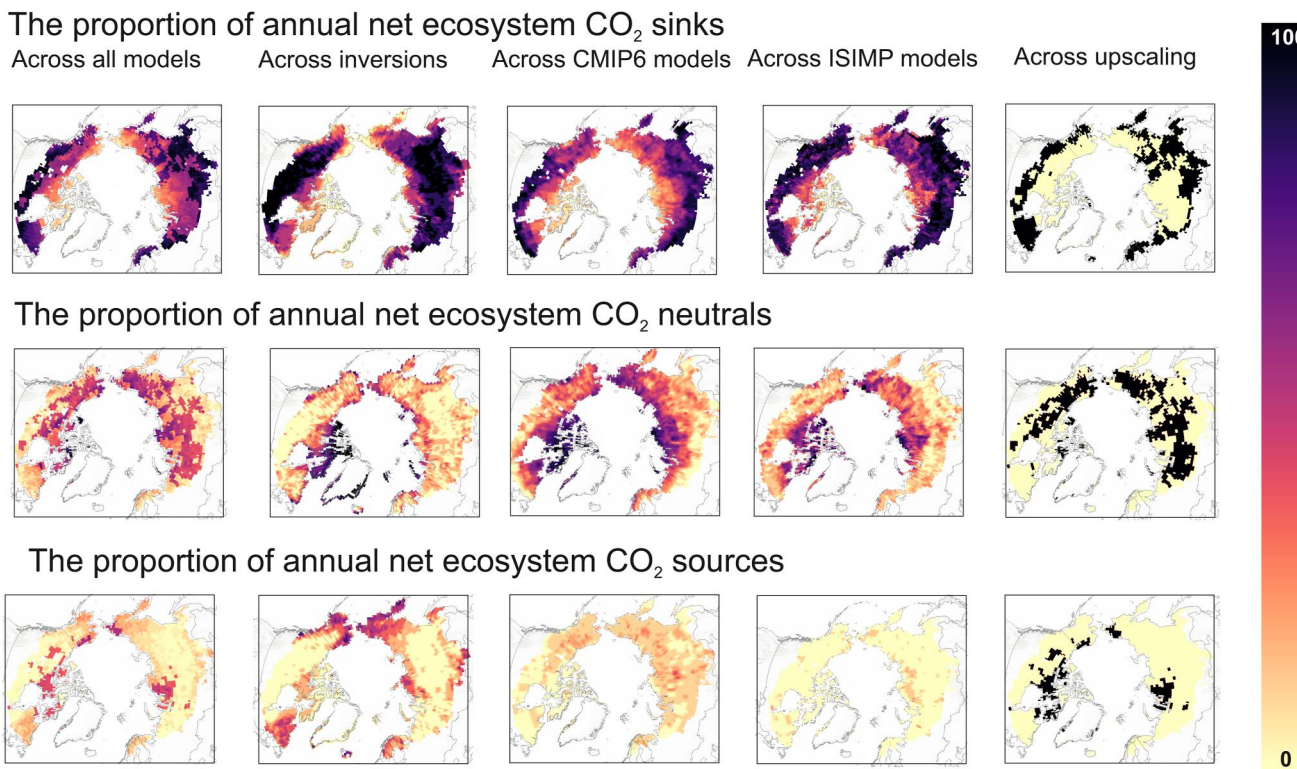


**Figure 6.** The proportion of models showing annual terrestrial net ecosystem CO<sub>2</sub> sinks ( $< -10 \text{ g C m}^{-2} \text{ yr}^{-1}$ ), CO<sub>2</sub> neutrals ( $-10 - +10 \text{ g C m}^{-2} \text{ yr}^{-1}$ ), and CO<sub>2</sub> sources ( $> +10 \text{ g C m}^{-2} \text{ yr}^{-1}$ ). The “Across all models” map was produced so that each modeling approach (inversions, process-based, and upscaling models) received equal weight. Note that inversion estimates include lake CO<sub>2</sub> fluxes as well, but fossil fuel emissions, cement carbonation sink, lateral fluxes and fire emissions have been removed; and the upscaling only includes one model and agreement cannot be calculated; thus values are either 0 (not a sink/neutral/source) or 100 (is a sink/neutral/source).

leading to an underestimation of the potential for C-climate feedbacks from these frozen soils. Only two of the CMIP6 models included a representation of permafrost C in soils (CESM and NorESM), which improved C stocks estimates in the permafrost region. The relatively short spin-up time of some models (on the order of centuries) compared to the slow build-up time of permafrost C over many millennia—especially for C-rich Pleistocene Yedoma deposits (Lindgren et al., 2018) and Holocene peatlands (Yu et al., 2010)—may be one reason for this underestimation (Huntzinger et al., 2020; Schwalm et al., 2019). Alternatively, inaccurate representations of vegetation cover and plant-derived C and nutrient inputs to the soil may also be responsible for low soil C stocks (Varney et al., 2022). Given the important role of soil C stocks in the permafrost C feedback, as well as the potential for C accumulation in soils with permafrost thaw (Treat et al., 2021), it is crucial to both simulate soil C stocks as well as demonstrate the potential for both soil C accumulation and loss.

Capturing vegetation dynamics is also critical to modeling permafrost dynamics but many dynamic global vegetation models (DGVMs; a type of LSMs that addresses the behavior and changes in vegetation) were originally developed to represent the biomes of lower latitudes where extreme winter conditions are absent (Bruhwiler et al., 2021; Lambert et al., 2022). The high degree of disagreement among models predicting future C balance in the permafrost region is attributed to uncertainty about whether plant productivity and subsequent ecosystem C uptake will compensate for permafrost C release (McGuire et al., 2018b). One limitation in the CMIP6 models was that only a few included vegetation dynamics (Canadell et al., 2021); those that did simulated Arctic grasses rather than dwarf shrubs and struggled to correctly simulate the seasonal trends of leaf area index (LAI; Song et al., 2021). In addition, accounting for nutrient limitations is essential to avoid an unrealistically strong vegetation response to CO<sub>2</sub> fertilization (Zaehle et al., 2015), but of the 11 land carbon cycle models used in CMIP6 ESMs, only six included a nitrogen cycle (Canadell et al., 2021).

Future model projections remain highly uncertain whether the permafrost region will act as a C source or sink (Braghieri et al., 2023). In addition to challenges with soils and vegetation, current LSMs miss the capability to

simulate abrupt changes following disturbances. While five of 11 models included in the land carbon cycle models used in CMIP6 ESMs simulated fire, none of them included fire-permafrost-carbon interactions (Canadell et al., 2021). Thermokarst processes are also absent although they can to a certain extent be represented in LSMs (N. D. Smith et al., 2022). Vegetation-specific disturbances such as insect outbreaks, frost damage, and droughts can affect the C balance (Reichstein et al., 2013), but improvements to vegetation dynamics should be priority. Furthermore, the contribution of peatland, inland aquatic ecosystems, and the lateral carbon fluxes between terrestrial and aquatic systems are not included in CMIP6 models but are included in regional modeling studies of C fluxes in the permafrost region (Chaudhary et al., 2020; Kicklighter et al., 2013; Lyu et al., 2018; McGuire et al., 2018a). The limited representation of processes is due to their complexity as well as the lack of observations integrating interactions between terrestrial and aquatic systems (Vonk et al., 2019). Overall, the potential for C sequestration in peatland and other soils (Treat et al., 2021), and other region-specific disturbances such as abrupt permafrost thaw (Turetsky et al., 2020) should be a major focus of future model development to achieve a more accurate quantification of the permafrost C feedback.

Progress in modeling wetland  $\text{CH}_4$  fluxes in high-latitude regions has been made over the past decades (Xiaofeng Xu, Yuan, et al., 2016). Site-scale validation of process-based LSMs suggest that models generally capture wetland  $\text{CH}_4$  variability well at seasonal and longer time scales but perform poorly at shorter time scales (<15 days; Zhen Zhang et al., 2023). Model-data comparisons show some issues with seasonality, including a strong underestimation of non-growing season (October-April)  $\text{CH}_4$  emissions by as much as two-thirds (Ito et al., 2023; Miller et al., 2016; Treat et al., 2018b; Xiyan Xu, Yuan, et al., 2016). Nevertheless, these data-model integration efforts do highlight that Arctic-boreal wetland  $\text{CH}_4$  processes are better captured than those in tropical wetlands (Delwiche et al., 2021; McNicol et al., 2023; Zhen Zhang et al., 2023).

Methane flux models still face challenges and uncertainties, particularly in defining the past and present extent of wetlands (Bloom et al., 2017; Peltola et al., 2019a; Saunois et al., 2020), capturing the spatial and temporal heterogeneity of wetland ecosystems in terms of soil moisture, inundation variability, including the vegetation communities, and predicting the effects of permafrost thaw on  $\text{CH}_4$  dynamics (Koven et al., 2011, 2015). These factors add uncertainty to data-driven flux upscaling and atmospheric inversions through *a priori* flux assumptions (Bruhwiler et al., 2021; Peltola et al., 2019a; Saunois et al., 2020). However, improvements in the recent wetland maps in Boreal-Arctic Wetland Lake Database (BAWLD) and Wetland Area and Dynamics for Methane Modeling (WAD2M) are promising (Olefeldt et al., 2021; Z. Zhang et al., 2021). Model intercomparisons have generated important maps and budget estimates of  $\text{CO}_2$  fluxes but are relatively uncommon for  $\text{CH}_4$  (Bloom et al., 2017; Collier et al., 2018; Ito et al., 2023; Melton et al., 2013), and should be undertaken as more models are developed. Challenges also remain for modeling  $\text{CH}_4$  cycling beyond the borders of wetlands, particularly in uplands and lakes. Uplands cover close to 80% of the permafrost region and can be both annual  $\text{CH}_4$  sources (Zona et al., 2016) and sinks (Oh et al., 2020; Voigt et al., 2023). Wetlands and lakes have differing  $\text{CH}_4$  emissions and processes (Kuhn et al., 2021b; Wik et al., 2016), but distinguishing these landforms in observations and remote sensing images can be difficult, leading to possible double counting of emissions sources (Thornton et al., 2016). Hybrid process modeling together with remote sensing and eddy covariance data have been used to estimate wetland  $\text{CH}_4$  fluxes relatively accurately (Watts et al., 2023), which incorporates important factors such as soil moisture, temperature, vegetation characteristics, and hydrological dynamics to estimate wetland  $\text{CH}_4$  fluxes.

Atmospheric inversion model ensembles are an integral part of determining global  $\text{CO}_2$  and  $\text{CH}_4$  budgets as they aggregate natural terrestrial and aquatic as well as anthropogenic sources over large domains (Friedlingstein et al., 2022; Saunois et al., 2020). Full ensembles have been less frequently used in the permafrost region where atmospheric inversions have a large model spread in  $\text{CO}_2$  and  $\text{CH}_4$  fluxes due to differing transport models, priors, and observations (Bruhwiler et al., 2021; Z. Liu et al., 2022). However, models are rapidly evolving. For example, airborne and satellite data are being more extensively used to define the prior estimates for inversions (Byrne et al., 2023; Tsuruta et al., 2023). While promising, satellite observations based on optical remote sensing still have some limitations for application during polar winter and with persistent cloud cover. Improvements should still be made toward better maps of surface conditions to better delineate flux surface fields (e.g., wetland distribution), an expanded tall tower network for better mixing ratio and isotopic data (Basu et al., 2022), and comprehensive sensitivity tests regarding transport modeling to understand Arctic-specific conditions (e.g., influence of polar vortex and shallow and stable boundary layers). Further iterations between top-down and bottom-up modeling informed and constrained by observational data have strong potential to resolve discrepancies in

permafrost C budgets (Commane et al., 2017; Elder et al., 2021; Miller et al., 2016); developments in model benchmarking systems and data assimilation will also help with furthering understanding and refining estimates (Collier et al., 2018; Y. Q. Luo et al., 2012; Stofferahn et al., 2019).

#### 4. Summary of the Next Steps

This review highlights significant progress in permafrost C cycle science since early permafrost maps and C flux syntheses (Tables 1 and 2). Major recent methodological advances include new geospatial data products describing permafrost conditions and soil C, nearly continuous records of CO<sub>2</sub> and CH<sub>4</sub> fluxes from eddy covariance towers across the permafrost domain, and the incorporation of permafrost-relevant characteristics into multiple process and machine-learning based models that can be used to simulate CO<sub>2</sub> and CH<sub>4</sub> fluxes. Several new key research topics have also emerged. Non-growing season emissions have a larger role in the annual C balance than previously thought, and even more so in a warmer climate. Vegetation shifts and enhanced productivity are key processes potentially mitigating positive permafrost climate feedbacks but might not always lead to increasing net annual C uptake because they can also alter soil microclimate and chemistry in a way that accelerates C emissions. Permafrost thaw is known to impact C cycling not only gradually but also abruptly, and in interaction with other disturbances, such as wildfires, will likely increase terrestrial C emissions to the atmosphere. For CH<sub>4</sub>, new hotspots such as thermogenic vents and craters as well as coldspots (areas with high uptake rates) are still being investigated. With the Arctic warming potentially up to four times faster than the global average (Rantanen et al., 2022), and permafrost thaw already happening faster than predicted in some parts of the region (Fewster et al., 2022), new processes and potentially novel ecosystems will likely emerge.

The integration of new process understanding from individual sites to cross-site data syntheses, and from individual models to model intercomparisons has been critical to estimating permafrost region C budgets and their trends. These data-model integration efforts have shown that while permafrost regions are cold and processes are slow, they still play a substantial role in the global C cycle. The permafrost region CH<sub>4</sub> budget ranges between 10 and 50 Tg CH<sub>4</sub> yr<sup>-1</sup>; trends over time remain uncertain due to the sparsity of data. The terrestrial CO<sub>2</sub> budget (a balance between GPP and ER) represents a relatively strong CO<sub>2</sub> sink (−700 to −100 Tg C yr<sup>-1</sup>), and there is evidence of both increasing growing season plant uptake and non-growing season C emissions. However, the partial disagreement across modeling approaches and syntheses, large spread of the estimated budgets, and unclear regional patterns and temporal trends shows fact that large uncertainties remain (Figures 4–6). The increased intensity and number of wildfires adds uncertainty to the evaluation of annual C balance in the permafrost region since a large fire year may offset multiple years of regional C uptake (M. W. Jones et al., 2022; Mack et al., 2021; X. J. Walker et al., 2019). Considering these challenges, we outline several research priorities below.

1. **Process-based knowledge:** Weather extremes and disturbances cause large inter-annual variability in C fluxes and change the contributions of the two key C fluxes—CO<sub>2</sub> and CH<sub>4</sub>—to the total C budget. At the same time, hydrological changes associated with permafrost thaw make understanding moisture gradients and terrestrial-aquatic interfaces more important to understand the controls of C cycling. As such, CO<sub>2</sub> and CH<sub>4</sub> exchange between ecosystems and the atmosphere do not capture the full response of permafrost C losses; lateral C fluxes also need to be quantified. New knowledge about extreme event impacts such as winter and summer droughts, fires, and insect outbreaks and their compound effects on C cycling derived from long-term field sites or controlled experiments targeting these extremes, and measurements in currently under-sampled drier upland landscapes and areas experiencing rapid disturbances, such as abrupt permafrost thaw, are crucial.
2. **Observations and syntheses:** While the network of sites with continuous observations is steadily increasing and subsequent data syntheses grow in scope (from 30 to 200 sites), detecting hotspots, hot moments, and long-term trends of *in-situ* CO<sub>2</sub> and CH<sub>4</sub> fluxes remains a challenge. Therefore, the observational network capacity must be increased to support the continuity of long-term eddy covariance CO<sub>2</sub> and CH<sub>4</sub> flux sites for year-round and long-term monitoring. New sites need to be established in areas where (a) data are currently lacking, such as in Russia and northern and eastern Canada, and (b) in areas experiencing disturbances. Chamber-based fluxes could be used to fill gaps in flux network data in remote locations but requires modeling to expand temporal coverage. The increasing availability of space-based CO<sub>2</sub> and CH<sub>4</sub> remote sensing data will address some of the spatial coverage challenges of the *in-situ* observation networks, but limitations remain for high latitudes. Finally, coordinated efforts are required to facilitate the creation of standardized and comprehensive terrestrial and aquatic CO<sub>2</sub> and CH<sub>4</sub> flux datasets and summaries for the permafrost region, improve inter-comparability of measurements and reduce latency in data collection, and to identify critical

data gaps (spatially and across ecosystem types). Further improvements to environmental data such as soil C, dominant plant species and their traits, and permafrost thaw status would help contextualize and upscale flux data.

3. **Modeling:** The three broad types of modeling approaches – statistical or machine learning-based upscaling, process modeling, and inversion approaches – are all needed to predict C fluxes in the permafrost domain. Process models are the most widely used technique to predict C fluxes but there are limitations related to cold-season emissions, belowground plant-soil feedbacks, permafrost thaw, disturbance history, as well as capturing temporal lags, tipping points, and non-linear responses. In addition, dynamic and spatially higher resolution wetland, soil moisture, and disturbance maps are needed to capture the rapidly changing permafrost landscapes, for example, the distribution of gradual and abrupt permafrost thaw. Using monitoring data to inform process-based and inversion models through data assimilation techniques could allow substantial decrease in model uncertainties (Y. Luo & Schuur, 2020). As more geospatial permafrost-related data products become available and new study sites are measured, better simulations and analyses of the dynamic processes that drive change in the permafrost region are possible.
4. **Model and data intercomparisons:** Regularly benchmarking and exploring the model-based magnitudes, trends, and drivers of C fluxes is necessary to identify areas of convergence and divergence between models and *in-situ* measurements (Collier et al., 2018). Determining whether key processes for the permafrost region identified by observations are included or adequately represented can significantly improve process-based model performance (Koven et al., 2011), as is identifying benchmarking metrics to constrain predictions (Schwalm et al., 2019). In particular, new CH<sub>4</sub> model intercomparisons are needed, especially as CH<sub>4</sub> models become more numerous and incorporate additional attributes. This ongoing evaluation will help improve our understanding and predictions of the permafrost region C fluxes.

#### Acknowledgments

We thank Jonas Vollmer for help with figure and table preparation, Bennet Juhls, Anna Irrgang, and two anonymous reviewers for comments that improved the manuscript, and Christian Rodenbeck, Frederic Chevallier, Yosuke Niwa, Junjie Liu, Liang Feng, and Ingrid Luijkx for providing the inversion outputs. Support for this study came from ERC Project FluxWIN (851181; CT, JH), Horizon Europe MISO Project (101086541; CT), Gordon and Betty Moore foundation (8414), the Audacious project (AMV, BMR, SMN, JDW), ESA AMPAC-Net Project (AMV, GH, JH), the IPAC working group of the International Permafrost Association (AMV, CT, SMN, JDW, BMR, EAGS), EU Horizon 2020 research and innovation programme (101003536; ESM2025 to EJB), the Joint UK BEIS/Defra Met Office Hadley Centre Climate Programme (GA01101 to EJB), ERC project Q-Arctic (951288 to MG), the Research Council of Norway (323945, 301639), and the Swedish Research Council VR (2022-04839 to GH). A portion of this work was carried out at the Jet Propulsion Laboratory, California Institute of Technology, under a contract with the National Aeronautics and Space Administration (80NM0018D0004). Additional support came from NASA Grant/Cooperative Agreement (NNX17AD69A to AC), U.S. Department of Energy (PNNL's LDRD program) and the Swiss National Science Foundation (project 200021\_215214) to AM, NSF PLR Arctic System Science RNA Permafrost Carbon Network (Grant 1931333; EAGS), and the Minderoo Foundation (EAGS). Open Access funding enabled and organized by Projekt DEAL.

While knowledge gaps remain, we anticipate the next decades to bring significant improvements in our process-level understanding and C budget estimates in the permafrost region. Continued coordinated efforts among the field, remote sensing, and modeling communities is required to integrate new knowledge throughout the knowledge chain from observations to modeling and predictions and finally to policy, and to most effectively constrain the permafrost region C budget (Fisher et al., 2018; Natali et al., 2022). Open data policies, reduced latency between observations and reporting, as well as improved methodological protocols, instrumentation and model intercomparisons need to be adopted moving forward. International networks addressing the permafrost region remain important, like the Permafrost Carbon Network and synthesis projects (Schuur et al., 2022), Arctic Monitoring and Assessment Program (AMAP) (Christensen et al., 2017), and RECCAPs (Ciais et al., 2022; McGuire et al., 2012) to understand and inform policy makers on ways to best protect and preserve these rapidly changing, sensitive permafrost ecosystems.

#### Data Availability Statement

We used data from open repositories for the regional analysis, including *in-situ* CO<sub>2</sub> and CH<sub>4</sub> flux data (Kuhn et al., 2021a; Treat et al., 2018a; Virkkala et al., 2021c) and upscaling outputs (Peltola et al., 2019b; Virkkala et al., 2021b). Specific details of the CMIP6 and ISIMIP model outputs used in the analyses can be found in Supporting Information S1 (Eyring et al., 2016; Frieler et al., 2017; Hugelius et al., 2023). Inversion outputs were published in Friedlingstein et al. (2022) and can be accessed by contacting Ingrid Luijkx ([ingrid.luijkx@wur.nl](mailto:ingrid.luijkx@wur.nl)).

#### References

Aalto, J., Karjalainen, O., Hjort, J., & Luoto, M. (2018). Statistical forecasting of current and future circum-arctic ground temperatures and active layer thickness. *Geophysical Research Letters*, 45(10), 4889–4898. <https://doi.org/10.1029/2018GL078007>

Alexandrov, G. A., Brovkin, V. A., & Kleinen, T. (2016). The influence of climate on peatland extent in Western Siberia since the last glacial maximum. *Scientific Reports*, 6(1), 24784. <https://doi.org/10.1038/srep24784>

Bartlett, K. B., & Harriss, R. C. (1993). Review and assessment of methane emissions from wetlands. *Chemosphere*, 26(1–4), 261–320. [https://doi.org/10.1016/0045-6535\(93\)90427-7](https://doi.org/10.1016/0045-6535(93)90427-7)

Bastviken, D., Treat, C. C., Pangala, S. R., Gauci, V., Enrich-Prast, A., Karlson, M., et al. (2022). The importance of plants for methane emission at the ecosystem scale. *Aquatic Botany*, 184, 103596. <https://doi.org/10.1016/j.aquabot.2022.103596>

Basu, S., Lan, X., Dlugokencky, E., Michel, S., Schwietzke, S., Miller, J. B., et al. (2022). Estimating emissions of methane consistent with atmospheric measurements of methane and 813C of methane. *Atmospheric Chemistry and Physics*, 22(23), 15351–15377. <https://doi.org/10.5194/acp-22-15351-2022>

Bellisario, L. M., Moore, T. R., & Bubier, J. L. (1998). Net ecosystem CO<sub>2</sub> exchange in a boreal peatland, northern Manitoba. *Ecoscience*, 5(4), 534–541. <https://doi.org/10.1080/11956860.1998.11682491>

Belshe, E. F., Schuur, E. A. G., & Bolker, B. M. (2013). Tundra ecosystems observed to be CO<sub>2</sub> sources due to differential amplification of the carbon cycle. *Ecology Letters*, 16(10), 1307–1315. <https://doi.org/10.1111/ele.12164>

Berner, L. T., Massey, R., Jantz, P., Forbes, B. C., Macias-Fauria, M., Myers-Smith, I., et al. (2020). Summer warming explains widespread but not uniform greening in the Arctic tundra biome. *Nature Communications*, 11(1), 4621. <https://doi.org/10.1038/s41467-020-18479-5>

Biskaborn, B. K., Smith, S. L., Noetzli, J., Matthes, H., Vieira, G., Streletskev, D. A., et al. (2019). Permafrost is warming at a global scale. *Nature Communications*, 10(1), 1–11. <https://doi.org/10.1038/s41467-018-08240-4>

Blodau, C. (2002). Carbon cycling in peatlands: A review of processes and controls. *Environmental Reviews*, 10(2), 111–134. <https://doi.org/10.1139/a02-004>

Bloom, A. A., Bowman, K. W., Lee, M., Turner, A. J., Schroeder, R., Worden, J. R., et al. (2017). A global wetland methane emissions and uncertainty dataset for atmospheric chemical transport models (WetCHARTs version 1.0). *Geoscience Model Development*, 10(6), 2141–2156. <https://doi.org/10.5194/gmd-10-2141-2017>

Bradshaw, C. J. A., & Warkentin, I. G. (2015). Global estimates of boreal forest carbon stocks and flux. *Global and Planetary Change*, 128, 24–30. <https://doi.org/10.1016/j.gloplacha.2015.02.004>

Braghiere, R. K., Fisher, J. B., Miner, K. R., Miller, C. E., Worden, J. R., Schimel, D. S., & Frankenberg, C. (2023). Tipping point in North American Arctic-Boreal carbon sink persists in new generation Earth system models despite reduced uncertainty. *Environmental Research Letters*, 18(2), 025008. <https://doi.org/10.1088/1748-9326/abc226>

Bridgman, S. D., Cadillo-Quiroz, H., Keller, J. K., & Zhuang, Q. (2013). Methane emissions from wetlands: Biogeochemical, microbial, and modeling perspectives from local to global scales. *Global Change Biology*, 19(5), 1325–1346. <https://doi.org/10.1111/gcb.12131>

Brosius, L. S., Anthony, K. M. W., Treat, C. C., Lenz, J., Jones, M. C., Bret-Harte, M. S., & Grosse, G. (2021). Spatiotemporal patterns of northern lake formation since the Last Glacial Maximum. *Quaternary Science Reviews*, 253, 106773. <https://doi.org/10.1016/j.quascirev.2020.106773>

Brown, J., Ferrians Jr, O. J., Heginbottom, J. A., Melnikov, E. S., & (Cartographer). (1998). Circum-Arctic map of permafrost and ground-ice conditions, revised 2001. National Snow and Ice Data Center. [https://doi.org/200021\\_215214](https://doi.org/200021_215214)

Bruhwiler, L., Basu, S., Butler, J. H., Chatterjee, A., Dlugokencky, E., Kenney, M. A., et al. (2021). Observations of greenhouse gases as climate indicators. *Climatic Change*, 165(1–2), 12. <https://doi.org/10.1007/s10584-021-03001-7>

Byrne, B., Baker, D. F., Basu, S., Bertolacci, M., Bowman, K. W., Carroll, D., et al. (2023). National CO<sub>2</sub> budgets (2015–2020) inferred from atmospheric CO<sub>2</sub> observations in support of the global stocktake. *Earth System Science Data*, 15(2), 963–1004. <https://doi.org/10.5194/essd-15-963-2023>

Canadell, J. G., Monteiro, P. M. S., Costa, M. H., Cotrim da Cunha, L., Cox, P. M., Eliseev, A. V., et al. (2021). Global carbon and other biogeochemical cycles and feedbacks. In V. Masson-Delmotte, P. Zhai, A. Pirani, S. L. Connors, C. Péan, S. Berger, et al. (Eds.), *Climate change 2021: The physical science basis. Contribution of working group I to the sixth assessment report of the intergovernmental panel on climate change* (pp. 673–816). Cambridge University Press.

Cassidy, A. E., Christen, A., & Henry, G. H. R. (2016). The effect of a permafrost disturbance on growing-season carbon-dioxide fluxes in a high Arctic tundra ecosystem. *Biogeosciences*, 13(8), 2291–2303. <https://doi.org/10.5194/bg-13-2291-2016>

Celis, G., Mauritz, M., Bracho, R., Salmon, V. G., Webb, E. E., Hutchings, J., et al. (2017). Tundra is a consistent source of CO<sub>2</sub> at a site with progressive permafrost thaw during 6 years of chamber and eddy covariance measurements. *Journal of Geophysical Research: Biogeosciences*, 122(6), 1471–1485. <https://doi.org/10.1002/2016JG003671>

Chadburn, S. E., Burke, E., Essery, R., Boike, J., Langer, M., Heikenfeld, M., et al. (2015). An improved representation of physical permafrost dynamics in the JULES land-surface model. *Geoscientific Model Development*, 8(5), 1493–1508. <https://doi.org/10.5194/gmd-8-1493-2015>

Chapin, F. S., BretHarte, M. S., Hobbie, S. E., & Zhong, H. L. (1996). Plant functional types as predictors of transient responses of arctic vegetation to global change. *Journal of Vegetation Science*, 7(3), 347–358. <https://doi.org/10.2307/32326278>

Chapin, F. S., McGuire, A. D., Randerson, J., Pielke, R., Baldocchi, D., Hobbie, S. E., et al. (2000). Arctic and boreal ecosystems of western North America as components of the climate system. *Global Change Biology*, 6(S1), 211–223. <https://doi.org/10.1046/j.1365-2486.2000.06022.x>

Chasmer, L., Cobaert, D., Mahoney, C., Millard, K., Peters, D., Devito, K., et al. (2020). Remote sensing of boreal wetlands 1: Data use for policy and management. *Remote Sensing*, 12(8), 1320. <https://doi.org/10.3390/rs12081320>

Chaudhary, N., Westermann, S., Lamba, S., Shurpali, N., Sannel, A. B. K., Schurgers, G., et al. (2020). Modelling past and future peatland carbon dynamics across the pan-Arctic. *Global Change Biology*, 26(7), 4119–4133. <https://doi.org/10.1111/gcb.15099>

Christensen, T. R., Panikov, N., Masteponov, M., Joabsson, A., Stewart, A., Oquist, M., et al. (2003). Biotic controls on CO<sub>2</sub> and CH<sub>4</sub> exchange in wetlands: A closed environment study. *Biogeochemistry*, 64(3), 337–354. <https://doi.org/10.1023/a:1024913730848>

Christensen, T. R., Rysgaard, S., Bendtsen, J., Else, B., Glud, R. N., Van Huissteden, J., et al. (2017). Arctic carbon cycling. In C. AMAP (Ed.), *Snow, water, ice and permafrost in the Arctic (SWIPA)* (pp. 203–218). Arctic Monitoring and Assessment Programme (AMAP).

Ciais, P., Bastos, A., Chevallier, F., Lauerwald, R., Poulter, B., Canadell, J. G., et al. (2022). Definitions and methods to estimate regional land carbon fluxes for the second phase of the regional carbon cycle assessment and processes project (RECCAP-2). *Geoscientific Model Development*, 15(3), 1289–1316. <https://doi.org/10.5194/gmd-15-1289-2022>

Clein, J. S., & Schimel, J. P. (1995). Microbial activity of tundra and taiga soils at subzero temperatures. *Soil Biology & Biochemistry*, 27(9), 1231–1234. [https://doi.org/10.1016/0038-0717\(95\)00044-f](https://doi.org/10.1016/0038-0717(95)00044-f)

Collier, N., Hoffman, F. M., Lawrence, D. M., Keppel-Aleks, G., Koven, C. D., Riley, W. J., et al. (2018). The international land model benchmarking (ILAMB) system: Design, theory, and implementation. *Journal of Advances in Modeling Earth Systems*, 10(11), 2731–2754. <https://doi.org/10.1029/2018MS001354>

Commane, R., Lindaas, J., Benmergui, J., Luus, K. A., Chang, R. Y.-W., Daube, B. C., et al. (2017). Carbon dioxide sources from Alaska driven by increasing early winter respiration from Arctic tundra. *Proceedings of the National Academy of Sciences*, 114(21), 5361–5366. <https://doi.org/10.1073/pnas.1618567114>

Dean, J. F., Middelburg, J. J., Röckmann, T., Aerts, R., Blauw, L. G., Egger, M., et al. (2018). Methane feedbacks to the global climate system in a warmer world. *Reviews of Geophysics*, 56(1), 207–250. <https://doi.org/10.1002/2017rg000559>

Delwiche, K. B., Knox, S. H., Malhotra, A., Fluet-Chouinard, E., McNicol, G., Feron, S., et al. (2021). FLUXNET-CH4: A global, multi-ecosystem dataset and analysis of methane seasonality from freshwater wetlands. *Earth System Science Data*, 13(7), 3607–3689. <https://doi.org/10.5194/essd-13-3607-2021>

Ekici, A., Beer, C., Hagemann, S., Boike, J., Langer, M., & Hauck, C. (2014). Simulating high-latitude permafrost regions by the JSBACH terrestrial ecosystem model. *Geoscientific Model Development*, 7(2), 631–647. <https://doi.org/10.5194/gmd-7-631-2014>

Elder, C. D., Thompson, D. R., Thorpe, A. K., Chandanpurkar, H. A., Hanke, P. J., Hasson, N., et al. (2021). Characterizing methane emission hotspots from thawing permafrost. *Global Biogeochemical Cycles*, 35(12), e2020GB006922. <https://doi.org/10.1029/2020GB006922>

Elmendorf, S. C., Henry, G. H. R., Hollister, R. D., Björk, R. G., Bjorkman, A. D., Callaghan, T. V., et al. (2012). Global assessment of experimental climate warming on tundra vegetation: Heterogeneity over space and time. *Ecology Letters*, 15(2), 164–175. <https://doi.org/10.1111/j.1461-0248.2011.01716.x>

Estop-Aragonés, C., Olefeldt, D., Abbott, B. W., Chanton, J. P., Czimczik, C. I., Dean, J. F., et al. (2020). Assessing the potential for mobilization of old soil carbon after permafrost thaw: A synthesis of 14C measurements from the northern permafrost region. *Global Biogeochemical Cycles*, 34(9), e2020GB006672. <https://doi.org/10.1029/2020GB006672>

Euskirchen, E. S., Edgar, C. W., Syndonia, B. H. M., Kade, A., Zimov, N., & Zimov, S. (2017). Interannual and seasonal patterns of carbon dioxide, water, and energy fluxes from ectonal and thermokarst-impacted ecosystems on carbon-rich permafrost soils in Northeastern Siberia. *Journal of Geophysical Research: Biogeosciences*, 122(10), 2651–2668. <https://doi.org/10.1002/2017JG004070>

Euskirchen, E. S., Edgar, C. W., Turetsky, M. R., Waldrop, M. P., & Harden, J. W. (2014). Differential response of carbon fluxes to climate in three peatland ecosystems that vary in the presence and stability of permafrost. *Journal of Geophysical Research: Biogeosciences*, 119(8), 1576–1595. <https://doi.org/10.1002/2014JG002683>

Eyring, V., Bony, S., Meehl, G. A., Senior, C. A., Stevens, B., Stouffer, R. J., & Taylor, K. E. (2016). Overview of the coupled model inter-comparison project phase 6 (CMIP6) experimental design and organization. *Geoscientific Model Development*, 9(5), 1937–1958. <https://doi.org/10.5194/gmd-9-1937-2016>

Fan, L., Wigneron, J. P., Ciais, P., Chave, J., Brandt, M., Sitch, S., et al. (2023). Siberian carbon sink reduced by forest disturbances. *Nature Geoscience*, 16(1), 56–62. <https://doi.org/10.1038/s41561-022-01087-x>

Farquharson, L. M., Romanovsky, V. E., Kholodov, A., & Nicolsky, D. (2022). Sub-aerial talik formation observed across the discontinuous permafrost zone of Alaska. *Nature Geoscience*, 15(6), 475–481. <https://doi.org/10.1038/s41561-022-00952-z>

Fewster, R. E., Morris, P. J., Ivanovic, R. F., Swindles, G. T., Peregon, A. M., & Smith, C. J. (2022). Imminent loss of climate space for permafrost peatlands in Europe and Western Siberia. *Nature Climate Change*, 12(4), 373–379. <https://doi.org/10.1038/s41558-022-01296-7>

Fisher, J. B., Hayes, D. J., Schwalm, C. R., Huntzinger, D. N., Stofferahn, E., Schaefer, K., et al. (2018). Missing pieces to modeling the Arctic-Boreal puzzle. *Environmental Research Letters*, 13(2), 020202. <https://doi.org/10.1088/1748-9326/aa9d9a>

Fisher, J. B., Huntzinger, D. N., Schwalm, C. R., & Sitch, S. (2014). Modeling the terrestrial biosphere. *Annual Review of Environment and Resources*, 39(1), 91–123. <https://doi.org/10.1146/annurev-environ-012913-093456>

Foster, A. C., Wang, J. A., Frost, G. V., Davidson, S. J., Hoy, E., Turner, K. W., et al. (2022). Disturbances in North American boreal forest and arctic tundra: Impacts, interactions, and responses. *Environmental Research Letters*, 17(11), 113001. <https://doi.org/10.1088/1748-9326/ac98d7>

Friedlingstein, P., Jones, M. W., O'Sullivan, M., Andrew, R. M., Bakker, D. C. E., Hauck, J., et al. (2022). Global Carbon Budget 2021. *Earth System Science Data*, 14(4), 1917–2005. <https://doi.org/10.5194/essd-14-1917-2022>

Friedrich, D., Hirnspurger, M., & Bauer, S. (Eds.) (2022). More than "nature, *Research on infrastructure and Settlements in the North*. LIT Verlag.

Frieler, K., Lange, S., Piontek, F., Reyer, C. P. O., Schwede, J., Warszawski, L., et al. (2017). Assessing the impacts of 1.5°C global warming: Simulation protocol of the inter-sectoral impact model intercomparison project (ISIMIP2b). *Geoscientific Model Development*, 10(12), 4321–4345. <https://doi.org/10.5194/gmd-10-4321-2017>

Frolking, S., & Roulet, N. T. (2007). Holocene radiative forcing impact of northern peatland carbon accumulation and methane emissions. *Global Change Biology*, 13(5), 1079–1088. <https://doi.org/10.1111/j.1365-2486.2007.01339.x>

Frolking, S., Talbot, J., Jones, M. C., Treat, C. C., Kauffman, J. B., Tuittila, E.-S., & Roulet, N. (2011). Peatlands in the Earth's 21st century climate systems. *Environmental Reviews*, 19(NA), 371–396. <https://doi.org/10.1139/A11-014>

Galera, L. d. A., Eckhardt, T., Beer, C., Pfeiffer, E.-M., & Knoblauch, C. (2023). Ratio of in situ CO<sub>2</sub> to CH<sub>4</sub> production and its environmental controls in polygonal tundra soils of Samoylov Island, Northeastern Siberia. *Journal of Geophysical Research: Biogeosciences*, 128(4), e2022JG006956. <https://doi.org/10.1029/2022JG006956>

Gorham, E., Lehman, C., Dyke, A., Janssens, J., & Dyke, L. (2007). Temporal and spatial aspects of peatland initiation following deglaciation in North America. *Quaternary Science Reviews*, 26(3–4), 300–311. <https://doi.org/10.1016/j.quascirev.2006.08.008>

Groendahl, L., Friberg, T., & Soegaard, H. (2007). Temperature and snow-melt controls on interannual variability in carbon exchange in the high Arctic. *Theoretical and Applied Climatology*, 88(1), 111–125. <https://doi.org/10.1007/s00704-005-0228-y>

Gruber, S. (2012). Derivation and analysis of a high-resolution estimate of global permafrost zonation. *The Cryosphere*, 6(1), 221–233. <https://doi.org/10.5194/tc-6-221-2012>

Gulev, S. K., Thorne, P. W., Ahn, J., Dentener, F. J., Domingues, C. M., Gerland, S., et al. (2021). Changing state of the climate system. In V. Masson-Delmotte, P. Zhai, A. Pirani, S. L. Connors, C. Péan, S. Berger, et al. (Eds.), *Climate change 2021: The physical science basis. Contribution of working group I to the sixth assessment report of the intergovernmental panel on climate change* (pp. 287–422). Cambridge University Press.

Harden, J. W., Koven, C. D., Ping, C.-L., Hugelius, G., McGuire, A. D., Camill, P., et al. (2012). Field information links permafrost carbon to physical vulnerabilities of thawing. *Geophysical Research Letters*, 39(15), L15704. <https://doi.org/10.1029/2012gl051958>

Harden, J. W., Manies, K. L., Turetsky, M. R., & Neff, J. C. (2006). Effects of wildfire and permafrost on soil organic matter and soil climate in interior Alaska. *Global Change Biology*, 12(12), 2391–2403. <https://doi.org/10.1111/j.1365-2486.2006.01255.x>

Harden, J. W., Sundquist, E. T., Stallard, R. F., & Mark, R. K. (1992). Dynamics of soil carbon during deglaciation of the Laurentide ice-sheet. *Science*, 258(5090), 1921–1924. <https://doi.org/10.1126/science.258.5090.1921>

Harris, S. A., French, H. M., Heginbottom, J. A., Johnston, G. H., Ladanyi, B., Sego, D. C., & Van Everdingen, R. O. (1988). Glossary of permafrost and related ground-ice terms (Technical Memorandum No. 142). *Retrieved from Ottawa*.

Hartley, I. P., Garnett, M. H., Sommerkorn, M., Hopkins, D. W., Fletcher, B. J., Sloan, V. L., et al. (2012). A potential loss of carbon associated with greater plant growth in the European Arctic. *Nature Climate Change*, 2(12), 875–879. <https://doi.org/10.1038/nclimate1575>

Hashemi, J., Zona, D., Arndt, K. A., Kalhori, A., & Oechel, W. C. (2021). Seasonality buffers carbon budget variability across heterogeneous landscapes in Alaskan Arctic tundra. *Environmental Research Letters*, 16(3), 035008. <https://doi.org/10.1088/1748-9326/abe2d1>

Hayes, D. J., Butman, D. E., Domke, G. M., Fisher, J. B., Neigh, C. S. R., & Welp, L. R. (2022). Chapter 6 - boreal forests. In B. Poulter, J. G. Canadell, D. J. Hayes, & R. L. Thompson (Eds.), *Balancing greenhouse gas budgets* (pp. 203–236). Elsevier. <https://doi.org/10.1016/b978-0-12-814952-2.00025-3>

Heijmans, M. M. P. D., Magnússon, R. Í., Lara, M. J., Frost, G. V., Myers-Smith, I. H., Van Huissteden, J., et al. (2022). Tundra vegetation change and impacts on permafrost. *Nature Reviews Earth & Environment*, 3(1), 68–84. <https://doi.org/10.1038/s43017-021-00233-0>

Helbig, M., Chasmer, L. E., Kljun, N., Quinton, W. L., Treat, C. C., & Sonnenstag, O. (2017). The positive net radiative greenhouse gas forcing of increasing methane emissions from a thawing boreal forest-wetland landscape. *Global Change Biology*, 23(6), 2413–2427. <https://doi.org/10.1111/gcb.13520>

Helbig, M., Živković, T., Alekseychik, P., Aurela, M., El-Madany, T. S., Euskirchen, E. S., et al. (2022). Warming response of peatland CO<sub>2</sub> sink is sensitive to seasonality in warming trends. *Nature Climate Change*, 12(8), 743–749. <https://doi.org/10.1038/s41558-022-01428-z>

Hengl, T., Mendes de Jesus, J., Heuvelink, G. B. M., Ruiperez Gonzalez, M., Kilibarda, M., Blagotić, A., et al. (2017). SoilGrids250m: Global gridded soil information based on machine learning. *Plos One*, 12(2), e0169748. <https://doi.org/10.1371/journal.pone.0169748>

Hewitt, R. E., Taylor, D. L., Genet, H., McGuire, A. D., & Mack, M. C. (2019). Below-ground plant traits influence tundra plant acquisition of newly thawed permafrost nitrogen. *Journal of Ecology*, 107(2), 950–962. <https://doi.org/10.1111/1365-2745.13062>

Hirst, C., Monhongval, A., Maucler, E., Thomas, M., Villani, M., Ledman, J., et al. (2023). Evidence for late winter biogeochemical connectivity in permafrost soils. *Communications Earth & Environment*, 4(1), 85. <https://doi.org/10.1038/s43247-023-00740-6>

Hiyama, T., Ueyama, M., Kotani, A., Iwata, H., Nakai, T., Okamura, M., et al. (2021). Lessons learned from more than a decade of greenhouse gas flux measurements at boreal forests in eastern Siberia and interior Alaska. *Polar Science*, 27, 100607. <https://doi.org/10.1016/j.polar.2020.100607>

Holloway, J. E., Lewkowicz, A. G., Douglas, T. A., Li, X., Turetsky, M. R., Baltzer, J. L., & Jin, H. (2020). Impact of wildfire on permafrost landscapes: A review of recent advances and future prospects. *Permafrost and Periglacial Processes*, 31(3), 371–382. <https://doi.org/10.1002/ppp.2048>

Hugelius, G., Bockheim, J. G., Camill, P., Elberling, B., Grosse, G., Harden, J. W., et al. (2013). A new data set for estimating organic carbon storage to 3 m depth in soils of the northern circumpolar permafrost region. *Earth System Science Data*, 5(2), 393–402. <https://doi.org/10.5194/essd-5-393-2013>

Hugelius, G., Loisel, J., Chadburn, S., Jackson, R. B., Jones, M., MacDonald, G., et al. (2020). Large stocks of peatland carbon and nitrogen are vulnerable to permafrost thaw. *Proceedings of the National Academy of Sciences*, 117(34), 20438–20446. <https://doi.org/10.1073/pnas.1916387117>

Hugelius, G., Ramage, J. L., Burke, E. J., Chatterjee, A., Smallman, T. L., Aalto, T., et al. (2023). Two decades of permafrost region CO<sub>2</sub>, CH<sub>4</sub>, and N<sub>2</sub>O budgets suggest a small net greenhouse gas source to the atmosphere. *ESS Open Archive*. <https://doi.org/10.22541/essoar.169444320.01914726/v1>

Hugelius, G., Strauss, J., Zubrzycki, S., Harden, J. W., Schuur, E. A. G., Ping, C. L., et al. (2014). Estimated stocks of circumpolar permafrost carbon with quantified uncertainty ranges and identified data gaps. *Biogeosciences*, 11(23), 6573–6593. <https://doi.org/10.5194/bg-11-6573-2014>

Huntzinger, D. N., Schaefer, K., Schwalm, C., Fisher, J. B., Hayes, D., Stofferahn, E., et al. (2020). Evaluation of simulated soil carbon dynamics in Arctic-Boreal ecosystems. *Environmental Research Letters*, 15(2), 025005. <https://doi.org/10.1088/1748-9326/ab6784>

IPCC. (2021). In J. M. Gutiérrez & A. M. Tréguier (Eds.), *Annex II: Models In V. Masson-Delmotte, P. Zhai, A. Pirani, S. L. Connors, C. Péan, S. Berger, N. Caud, Y. Chen, L. Goldfarb, M. I. Gomis, M. Huang, K. Leitzell, E. Lonnoy, J. B. R. Matthews, T. K. Maycock, T. Waterfield, O. Yelekçi, R. Yu, & B. Zhou (Eds.), climate change 2021: The physical science basis. Contribution of working group I to the sixth assessment report of the intergovernmental panel on climate change* (pp. 2087–2138). Cambridge University Press.

Ito, A., Li, T., Qin, Z., Melton, J. R., Tian, H., Kleinen, T., et al. (2023). Cold-season methane fluxes simulated by GCP-CH4 Models. *Geophysical Research Letters*, 50(14), e2023GL103037. <https://doi.org/10.1029/2023GL103037>

Jones, M. C., Grosse, G., Treat, C., Turetsky, M., Anthony, K. W., & Brosius, L. (2023). Past permafrost dynamics can inform future permafrost carbon-climate feedbacks. *Communications Earth & Environment*, 4(1), 272. <https://doi.org/10.1038/s43247-023-00886-3>

Jones, M. C., Harden, J., O'Donnell, J., Manies, K., Jorgenson, T., Treat, C., & Ewing, S. (2017). Rapid carbon loss and slow recovery following permafrost thaw in boreal peatlands. *Global Change Biology*, 23(3), 1109–1127. <https://doi.org/10.1111/gcb.13403>

Jones, M. W., Abatzoglou, J. T., Veraverbeke, S., Andela, N., Lasslop, G., Forkel, M., et al. (2022). Global and regional trends and drivers of fire under climate change. *Reviews of Geophysics*, 60(3), e2020RG000726. <https://doi.org/10.1029/2020RG000726>

Jorgensen, C. J., Johansen, K. M. L., Westergaard-Nielsen, A., & Elberling, B. (2015). Net regional methane sink in high arctic soils of northeast Greenland. *Nature Geoscience*, 8(1), 20–23. <https://doi.org/10.1038/ngeo2305>

Jorgenson, M. T., & Osterkamp, T. E. (2005). Response of boreal ecosystems to varying modes of permafrost degradation. *Canadian Journal of Forest Research-Revue Canadienne De Recherche Forestiere*, 35(9), 2100–2111. <https://doi.org/10.1139/X05-153>

Jorgenson, M. T., Shur, Y. L., & Pullman, E. R. (2006). Abrupt increase in permafrost degradation in Arctic Alaska. *Geophysical Research Letters*, 33(2), L02503. <https://doi.org/10.1029/2005GL024960>

Jung, M., Schwalm, C., Migliavacca, M., Walther, S., Camps-Valls, G., Koirala, S., et al. (2020). Scaling carbon fluxes from eddy covariance sites to globe: Synthesis and evaluation of the FLUXCOM approach. *Biogeosciences*, 17(5), 1343–1365. <https://doi.org/10.5194/bg-17-1343-2020>

Karesdotter, E., Destouni, G., Ghajarnia, N., Hugelius, G., & Kalantari, Z. (2021). Mapping the vulnerability of Arctic wetlands to global warming. *Earth's Future*, 9(5). <https://doi.org/10.1029/2020ef001858>

Keuper, F., Wild, B., Kummu, M., Beer, C., Blume-Werry, G., Fontaine, S., et al. (2020). Carbon loss from northern circumpolar permafrost soils amplified by rhizosphere priming. *Nature Geoscience*, 13(8), 560–565. <https://doi.org/10.1038/s41561-020-0607-0>

Kicklighter, D. W., Hayes, D. J., McClelland, J. W., Peterson, B. J., McGuire, A. D., & Melillo, J. M. (2013). Insights and issues with simulating terrestrial DOC loading of Arctic river networks. *Ecological Applications*, 23(8), 1817–1836. <https://doi.org/10.1890/11-1050.1>

Kim, J., Kim, Y., Zona, D., Oechel, W., Park, S.-J., Lee, B.-Y., et al. (2021). Carbon response of tundra ecosystems to advancing greenup and snowmelt in Alaska. *Nature Communications*, 12(1), 6879. <https://doi.org/10.1038/s41467-021-26876-7>

Kim, Y., Kimball, J. S., Zhang, K., & McDonald, K. C. (2012). Satellite detection of increasing Northern Hemisphere non-frozen seasons from 1979 to 2008: Implications for regional vegetation growth. *Remote Sensing of Environment*, 121, 472–487. <https://doi.org/10.1016/j.rse.2012.02.014>

Kittler, F., Heimann, M., Kolle, O., Zimov, N., Zimov, S., & Gockede, M. (2017). Long-term drainage reduces CO<sub>2</sub> uptake and CH<sub>4</sub> emissions in a Siberian permafrost ecosystem. *Global Biogeochemical Cycles*, 31(12), 1704–1717. <https://doi.org/10.1002/2017gb005774>

Kleber, G. E., Hodson, A. J., Magerl, L., Mannerfelt, E. S., Bradbury, H. J., Zhu, Y. Z., et al. (2023). Groundwater springs formed during glacial retreat are a large source of methane in the high Arctic. *Nature Geoscience*, 16(7), 597–604. <https://doi.org/10.1038/s41561-023-01210-6>

Klotz, L. A., Sonnentag, O., Wang, Z., Wang, J. A., & Kang, M. (2023). Oil and natural gas wells across the NASA ABoVE domain: Fugitive methane emissions and broader environmental impacts. *Environmental Research Letters*, 18(3), 035008. <https://doi.org/10.1088/1748-9326/abe52>

Knox, S. H., Jackson, R. B., Poulter, B., McNicol, G., Fluet-Chouinard, E., Zhang, Z., et al. (2019). FLUXNET-CH4 synthesis activity: Objectives, observations, and future directions. *Bulletin of the American Meteorological Society*, 100(12), 2607–2632. <https://doi.org/10.1175/bams-d-18-0268.1>

Kohnert, K., Serafimovich, A., Metzger, S., Hartmann, J., & Sachs, T. (2017). Strong geologic methane emissions from discontinuous terrestrial permafrost in the Mackenzie Delta, Canada. *Scientific Reports*, 7(1), 5828. <https://doi.org/10.1038/s41598-017-05783-2>

Koven, C. D., Lawrence, D. M., & Riley, W. J. (2015). Permafrost carbon–climate feedback is sensitive to deep soil carbon decomposability but not deep soil nitrogen dynamics. *Proceedings of the National Academy of Sciences*, 112(12), 3752–3757. <https://doi.org/10.1073/pnas.1415123112>

Koven, C. D., Ringeval, B., Friedlingstein, P., Ciais, P., Cadule, P., Khvorostyanov, D., et al. (2011). Permafrost carbon–climate feedbacks accelerate global warming. *Proceedings of the National Academy of Sciences*, 108(36), 14769–14774. <https://doi.org/10.1073/pnas.1103910108>

Kuhn, M. A., Varner, R., Bastviken, D., Crill, P., MacIntyre, S., Turetsky, M. R., et al. (2021a). BAWLD-CH4: Methane fluxes from boreal and arctic ecosystems [Dataset]. *Arctic Data Center*. <https://doi.org/10.18739/A2DN3ZX1R>

Kuhn, M. A., Varner, R. K., Bastviken, D., Crill, P., MacIntyre, S., Turetsky, M., et al. (2021b). BAWLD-CH4: A comprehensive dataset of methane fluxes from boreal and arctic ecosystems. *Earth System Science Data*, 13(11), 5151–5189. <https://doi.org/10.5194/essd-13-5151-2021>

Lai, D. Y. F. (2009). Methane dynamics in northern peatlands: A review. *Pedosphere*, 19(4), 409–421. [https://doi.org/10.1016/S1002-0160\(09\)0003-4](https://doi.org/10.1016/S1002-0160(09)0003-4)

Lambert, M. S. A., Tang, H., Aas, K. S., Stordal, F., Fisher, R. A., Fang, Y., et al. (2022). Inclusion of a cold hardening scheme to represent frost tolerance is essential to model realistic plant hydraulics in the Arctic–boreal zone in CLM5.0-FATES-Hydro. *Geoscientific Model Development*, 15(23), 8809–8829. <https://doi.org/10.5194/gmd-15-8809-2022>

Lange, S. (2019). Trend-preserving bias adjustment and statistical downscaling with ISIMIP3BASD (v1.0). *Geoscientific Model Development*, 12(7), 3055–3070. <https://doi.org/10.5194/gmd-12-3055-2019>

Lawrence, D. M., Slater, A. G., & Swenson, S. C. (2012). Simulation of present-day and future permafrost and seasonally frozen ground conditions in CCSM4. *Journal of Climate*, 25(7), 2207–2225. <https://doi.org/10.1175/jcli-d-11-00334.1>

Le Mer, J., & Roger, P. (2001). Production, oxidation, emission and consumption of methane by soils: A review. *European Journal of Soil Biology*, 37(1), 25–50. [https://doi.org/10.1016/S1164-5563\(01\)01067-6](https://doi.org/10.1016/S1164-5563(01)01067-6)

Li, X.-Y., Jin, H.-J., Wang, H.-W., Marchenko, S. S., Shan, W., Luo, D.-L., et al. (2021). Influences of forest fires on the permafrost environment: A review. *Advances in Climate Change Research*, 12(1), 48–65. <https://doi.org/10.1016/j.accre.2021.01.001>

Li, Z.-L., Mu, C.-C., Chen, X., Wang, X.-Y., Dong, W.-W., Jia, L., et al. (2021). Changes in net ecosystem exchange of CO<sub>2</sub> in Arctic and their relationships with climate change during 2002–2017. *Advances in Climate Change Research*, 12(4), 475–481. <https://doi.org/10.1016/j.accre.2021.06.004>

Lindgren, A., Hugelius, G., & Kuhry, P. (2018). Extensive loss of past permafrost carbon but a net accumulation into present-day soils. *Nature*, 560(7717), 219–222. <https://doi.org/10.1038/s41586-018-0371-0>

Liu, C. X., Huang, H. B., & Sun, F. D. (2021). A pixel-based vegetation greenness trend analysis over the Russian tundra with all available landsat data from 1984 to 2018. *Remote Sensing*, 13(23), 15. <https://doi.org/10.3390/rs13234933>

Liu, Z., Kimball, J. S., Ballantyne, A. P., Parazoo, N. C., Wang, W. J., Bastos, A., et al. (2022). Respiratory loss during late-growing season determines the net carbon dioxide sink in northern permafrost regions. *Nature Communications*, 13(1), 5626. <https://doi.org/10.1038/s41467-022-33293-x>

López-Blanco, E., Exbrayat, J. F., Lund, M., Christensen, T. R., Tamstorf, M. P., Slevin, D., et al. (2019). Evaluation of terrestrial pan-Arctic carbon cycling using a data-assimilation system. *Earth System Dynamics*, 10(2), 233–255. <https://doi.org/10.5194/esd-10-233-2019>

Lund, M., Lafleur, P. M., Roulet, N. T., Lindroth, A., Christensen, T. R., Aurela, M., et al. (2010). Variability in exchange of CO<sub>2</sub> across 12 northern peatland and tundra sites. *Global Change Biology*, 16(9), 2436–2448. <https://doi.org/10.1111/j.1365-2486.2009.02104.x>

Lund, M., Raundrup, K., Westergaard-Nielsen, A., López-Blanco, E., Nyman, J., & Aastrup, P. (2017). Larval outbreaks in West Greenland: Instant and subsequent effects on tundra ecosystem productivity and CO<sub>2</sub> exchange. *Ambio*, 46(1), 26–38. <https://doi.org/10.1007/s13280-016-0863-9>

Luo, Y., & Schuur, E. A. G. (2020). Model parameterization to represent processes at unresolved scales and changing properties of evolving systems. *Global Change Biology*, 26(3), 1109–1117. <https://doi.org/10.1111/gcb.14939>

Luo, Y. Q., Randerson, J. T., Abramowitz, G., Bacour, C., Blyth, E., Carvalhais, N., et al. (2012). A framework for benchmarking land models. *Biogeosciences*, 9(10), 3857–3874. <https://doi.org/10.5194/bg-9-3857-2012>

Lyu, Z., Genet, H., He, Y. J., Zhuang, Q. L., McGuire, A. D., Bennett, A., et al. (2018). The role of environmental driving factors in historical and projected carbon dynamics of wetland ecosystems in Alaska. *Ecological Applications*, 28(6), 1377–1395. <https://doi.org/10.1002/ea.1755>

Mack, M. C., Walker, X. J., Johnstone, J. F., Alexander, H. D., Melvin, A. M., Jean, M., & Miller, S. N. (2021). Carbon loss from boreal forest wildfires offset by increased dominance of deciduous trees. *Science*, 372(6539), 280–283. <https://doi.org/10.1126/science.abf3903>

Malhotra, A., Todd-Brown, K., Nave, L. E., Batjes, N. H., Holmquist, J. R., Hoyt, A. M., et al. (2019). The landscape of soil carbon data: Emerging questions, synergies and databases. *Progress in Physical Geography: Earth and Environment*, 43(5), 707–719. <https://doi.org/10.1177/030913319873309>

Matthews, E., & Fung, I. (1987). Methane emission from natural wetlands: Global distribution, area, and environmental characteristics of sources. *Global Biogeochemical Cycles*, 1(1), 61–86. <https://doi.org/10.1029/GB001i001p00061>

McGuire, A. D., Anderson, L. G., Christensen, T. R., Dallimore, S., Guo, L. D., Hayes, D. J., et al. (2009). Sensitivity of the carbon cycle in the Arctic to climate change. *Ecological Monographs*, 79(4), 523–555. <https://doi.org/10.1890/08-2025.1>

McGuire, A. D., Christensen, T. R., Hayes, D., Heroult, A., Euskirchen, E., Kimball, J. S., et al. (2012). An assessment of the carbon balance of Arctic tundra: Comparisons among observations, process models, and atmospheric inversions. *Biogeosciences*, 9(8), 3185–3204. <https://doi.org/10.5194/bg-9-3185-2012>

McGuire, A. D., Genet, H., Lyu, Z., Pastick, N., Stackpoole, S., Birdsey, R., et al. (2018a). Assessing historical and projected carbon balance of Alaska: A synthesis of results and policy/management implications. *Ecological Applications*, 28(6), 1396–1412. <https://doi.org/10.1002/ea.1768>

McGuire, A. D., Koven, C., Lawrence, D. M., Clein, J. S., Xia, J., Beer, C., et al. (2016). Variability in the sensitivity among model simulations of permafrost and carbon dynamics in the permafrost region between 1960 and 2009. *Global Biogeochemical Cycles*, 30(7), 1015–1037. <https://doi.org/10.1002/2016GB005405>

McGuire, A. D., Lawrence, D. M., Koven, C., Clein, J. S., Burke, E., Chen, G., et al. (2018b). Dependence of the evolution of carbon dynamics in the northern permafrost region on the trajectory of climate change. *Proceedings of the National Academy of Sciences*, 115(15), 3882–3887. <https://doi.org/10.1073/pnas.1719903115>

McNicol, G., Fluet-Chouinard, E., Ouyang, Z., Knox, S., Zhang, Z., Aalto, T., et al. (2023). Upscaling wetland methane emissions from the FLUXNET-CH4 Eddy covariance network (UpCH4 v1.0): Model development, network assessment, and budget comparison. *AGU Advances*, 4(5), e2023AV000956. <https://doi.org/10.1029/2023AV000956>

Mekonnen, Z. A., Riley, W. J., Berner, L. T., Bouskill, N. J., Torn, M. S., Iwahana, G., et al. (2021). Arctic tundra shrubification: A review of mechanisms and impacts on ecosystem carbon balance. *Environmental Research Letters*, 16(5), 28. <https://doi.org/10.1088/1748-9326/abf28b>

Melton, J. R., Wania, R., Hodson, E. L., Poulter, B., Ringeval, B., Spahni, R., et al. (2013). Present state of global wetland extent and wetland methane modelling: Conclusions from a model inter-comparison project (WETCHIMP). *Biogeosciences*, 10(2), 753–788. <https://doi.org/10.5194/bg-10-753-2013>

Meredith, M., Sommernorn, M., Cassotta, S., Derksen, C., Ekaykin, A., Hollowed, A. B., et al. (2019). *Polar regions*. Cambridge.

Miller, S. M., Miller, C. E., Commane, R., Chang, R. Y. W., Dinardo, S. J., Henderson, J. M., et al. (2016). A multiyear estimate of methane fluxes in Alaska from CARVE atmospheric observations. *Global Biogeochemical Cycles*, 30(10), 1441–1453. <https://doi.org/10.1002/2016GB005419>

Miner, K. R., Turetsky, M. R., Malina, E., Bartsch, A., Tamminen, J., McGuire, A. D., et al. (2022). Permafrost carbon emissions in a changing Arctic. *Nature Reviews Earth & Environment*, 3(1), 55–67. <https://doi.org/10.1038/s43017-021-00230-3>

Mishra, U., Hugelius, G., Shelef, E., Yang, Y., Strauss, J., Lupachev, A., et al. (2021). Spatial heterogeneity and environmental predictors of permafrost region soil organic carbon stocks. *Science Advances*, 7(9), eaaz5236. <https://doi.org/10.1126/sciadv.aaz5236>

Myers-Smith, I. H., Kerby, J. T., Phoenix, G. K., Bjerke, J. W., Epstein, H. E., Assmann, J. J., et al. (2020). Complexity revealed in the greening of the Arctic. *Nature Climate Change*, 10(2), 106–117. <https://doi.org/10.1038/s41558-019-0688-1>

Natali, S. M., Bronen, R., Cochran, P., Holdren, J. P., Rogers, B. M., & Treharne, R. (2022). Incorporating permafrost into climate mitigation and adaptation policy. *Environmental Research Letters*, 17(9), 091001. <https://doi.org/10.1088/1748-9326/ac8e5a>

Natali, S. M., Watts, J. D., Rogers, B. M., Potter, S., Ludwig, S. M., Selbmann, A.-K., et al. (2019). Large loss of CO<sub>2</sub> in winter observed across the northern permafrost region. *Nature Climate Change*, 9(11), 852–857. <https://doi.org/10.1038/s41558-019-0592-8>

Nicolksy, D. J., Romanovsky, V. E., Alexeev, V. A., & Lawrence, D. M. (2007). Improved modeling of permafrost dynamics in a GCM land-surface scheme. *Geophysical Research Letters*, 34(8). <https://doi.org/10.1029/2007gl029525>

Nilsson, M., Mikkel, C., Sundh, I., Granberg, G., Svensson, B. H., & Ranneby, B. (2001). Methane emission from Swedish mires: National and regional budgets and dependence on mire vegetation. *Journal of Geophysical Research*, 106(D18), 20847–20860. <https://doi.org/10.1029/2001jd900119>

Nitze, I., Grosse, G., Jones, B. M., Romanovsky, V. E., & Boike, J. (2018). Remote sensing quantifies widespread abundance of permafrost region disturbances across the Arctic and Subarctic. *Nature Communications*, 9(1), 5423. <https://doi.org/10.1038/s41467-018-07663-3>

Obu, J. (2021). How much of the Earth's surface is underlain by permafrost? *Journal of Geophysical Research: Earth Surface*, 126(5), e2021JF006123. <https://doi.org/10.1029/2021JF006123>

Obu, J., Westermann, S., Bartsch, A., Berdnikov, N., Christiansen, H. H., Dashtseren, A., et al. (2019). Northern Hemisphere permafrost map based on TTOP modelling for 2000–2016 at 1 km<sup>2</sup> scale. *Earth-Science Reviews*, 193, 299–316. <https://doi.org/10.1016/j.earscirev.2019.04.023>

Oh, Y., Zhuang, Q., Liu, L., Welp, L. R., Lau, M. C. Y., Onstott, T. C., et al. (2020). Reduced net methane emissions due to microbial methane oxidation in a warmer Arctic. *Nature Climate Change*, 10(4), 317–321. <https://doi.org/10.1038/s41558-020-0734-z>

Olefeldt, D., Euskirchen, E. S., Harden, J., Kane, E., McGuire, A. D., Waldrop, M. P., & Turetsky, M. R. (2017). A decade of boreal rich fen greenhouse gas fluxes in response to natural and experimental water table variability. *Global Change Biology*, 23(6), 2428–2440. <https://doi.org/10.1111/gcb.13612>

Olefeldt, D., Goswami, S., Grosse, G., Hayes, D., Hugelius, G., Kuhry, P., et al. (2016). Circumpolar distribution and carbon storage of thermokarst landscapes. *Nature Communications*, 7(1), 13043. <https://doi.org/10.1038/ncomms13043>

Olefeldt, D., Hovemyr, M., Kuhn, M. A., Bastviken, D., Bohn, T. J., Connolly, J., et al. (2021). The boreal-Arctic wetland and lake dataset (BAWLD). *Earth System Science Data*, 13(11), 5127–5149. <https://doi.org/10.5194/essd-13-5127-2021>

Olefeldt, D., Roulet, N. T., Bergeron, O., Crill, P., Bæckstrand, K., & Christensen, T. R. (2012). Net carbon accumulation of a high-latitude permafrost palsu mira similar to permafrost-free peatlands. *Geophysics Research Letter*, 39(3), L03501. <https://doi.org/10.1029/2011gl050355>

Olefeldt, D., Turetsky, M. R., Crill, P. M., & McGuire, A. D. (2013). Environmental and physical controls on northern terrestrial methane emissions across permafrost zones. *Global Change Biology*, 19(2), 589–603. <https://doi.org/10.1111/gcb.12071>

O'Neill, H. B., Wolfe, S. A., & Duchesne, C. (2019). New ground ice maps for Canada using a paleogeographic modelling approach. *The Cryosphere*, 13(3), 753–773. <https://doi.org/10.5194/tc-13-753-2019>

Öquist, M. G., Sparrman, T., Klemedtsson, L., Drotz, S. H., Grip, H., Schleucher, J., & Nilsson, M. (2009). Water availability controls microbial temperature responses in frozen soil CO<sub>2</sub> production. *Global Change Biology*, 15(11), 2715–2722. <https://doi.org/10.1111/j.1365-2486.2009.01898.x>

Osterkamp, T. E., & Romanovsky, V. E. (1999). Evidence for warming and thawing of discontinuous permafrost in Alaska. *Permafrost and Periglacial Processes*, 10(1), 17–37. [https://doi.org/10.1002/\(sici\)1099-1530\(199901/03\)10:1<17::aid-ppp303>3.0.co;2-4](https://doi.org/10.1002/(sici)1099-1530(199901/03)10:1<17::aid-ppp303>3.0.co;2-4)

Outcalt, S. I., Nelson, F. E., & Hinkel, K. M. (1990). The zero-curtain effect: Heat and mass transfer across an isothermal region in freezing soil. *Water Resources Research*, 26(7), 1509–1516. <https://doi.org/10.1029/WR026i007p01509>

Overduin, P. P., Schneider von Deimling, T., Miesner, F., Grigoriev, M. N., Ruppel, C., Vasiliev, A., et al. (2019). Submarine permafrost map in the Arctic modeled using 1-D transient heat flux (SuPerMAP). *Journal of Geophysical Research: Oceans*, 124(6), 3490–3507. <https://doi.org/10.1029/2018JC014675>

Overeem, I., Nienhuis, J. H., & Piliouras, A. (2022). Ice-dominated arctic deltas. *Nature Reviews Earth & Environment*, 3(4), 225–240. <https://doi.org/10.1038/s43017-022-00268-x>

Pallandt, M. M. T. A., Kumar, J., Mauritz, M., Schuur, E. A. G., Virkkala, A. M., Celis, G., et al. (2022). Representativeness assessment of the pan-Arctic eddy covariance site network and optimized future enhancements. *Biogeosciences*, 19(3), 559–583. <https://doi.org/10.5194/bg-19-559-2022>

Palmtag, J., Obu, J., Kuhry, P., Richter, A., Siewert, M. B., Weiss, N., et al. (2022). A high spatial resolution soil carbon and nitrogen dataset for the northern permafrost region based on circumpolar land cover upscaling. *Earth System Science Data*, 14(9), 4095–4110. <https://doi.org/10.5194/essd-14-4095-2022>

Payette, S., Delwaide, A., Caccianiga, M., & Beauchemin, M. (2004). Accelerated thawing of subarctic peatland permafrost over the last 50 years. *Geophysical Research Letters*, 31(18), L18208. <https://doi.org/10.1029/2004GL020358>

Pedron, S. A., Welker, J. M., Euskirchen, E. S., Klein, E. S., Walker, J. C., Xu, X., & Czimczik, C. I. (2022). Closing the winter gap—Year-round measurements of soil CO<sub>2</sub> emission sources in arctic tundra. *Geophysical Research Letters*, 49(6), e2021GL097347. <https://doi.org/10.1029/2021GL097347>

Peltola, O., Vesala, T., Gao, Y., Räty, O., Alekseychik, P., Aurela, M., et al. (2019a). Monthly gridded data product of northern wetland methane emissions based on upscaling eddy covariance observations. *Earth System Science Data*, 11(3), 1263–1289. <https://doi.org/10.5194/essd-11-1263-2019>

Peltola, O., Vesala, T., Gao, Y., Räty, O., Alekseychik, P., Aurela, M., et al. (2019b). Dataset for "monthly gridded data product of northern wetland methane emissions based on upscaling eddy covariance observations" [Dataset]. *Zenodo*. <https://doi.org/10.5281/zenodo.3247295>

Peng, S., Lin, X., Thompson, R. L., Xi, Y., Liu, G., Hauglustaine, D., et al. (2022). Wetland emission and atmospheric sink changes explain methane growth in 2020. *Nature*, 612(7940), 477–482. <https://doi.org/10.1038/s41586-022-05447-w>

Pirk, N., Sievers, J., Mertes, J., Parmentier, F. J. W., Mastepanov, M., & Christensen, T. R. (2017). Spatial variability of CO<sub>2</sub> uptake in polygonal tundra: Assessing low-frequency disturbances in eddy covariance flux estimates. *Biogeosciences*, 14(12), 3157–3169. <https://doi.org/10.5194/bg-14-3157-2017>

Plaza, C., Pegoraro, E., Bracho, R., Celis, G., Crummer, K. G., Hutchings, J. A., et al. (2019). Direct observation of permafrost degradation and rapid soil carbon loss in tundra. *Nature Geoscience*, 12(8), 627–631. <https://doi.org/10.1038/s41561-019-0387-6>

Poggio, L., De Sousa, L. M., Batjes, N. H., Heuvelink, G. B. M., Kempen, B., Ribeiro, E., & Rossiter, D. (2021). SoilGrids 2.0: Producing soil information for the globe with quantified spatial uncertainty. *SOIL*, 7(1), 217–240. <https://doi.org/10.5194/soil-7-217-2021>

Ramage, J. L., Kuhn, M., Virkkala, A.-M., Voigt, C., Marushchak, M. E., Bastos, A., et al. (2023). The net GHG balance and budget of the permafrost region (2000–2020) from ecosystem flux upscaling. *ESS Open Archive*, 29. <https://doi.org/10.22541/essoar.169462008.85493456/v1>

Ran, Y., Li, X., Cheng, G., Che, J., Aalto, J., Karjalainen, O., et al. (2022). New high-resolution estimates of the permafrost thermal state and hydrothermal conditions over the Northern Hemisphere. *Earth System Science Data*, 14(2), 865–884. <https://doi.org/10.5194/essd-14-865-2022>

Rantanen, M., Karpeckho, A. Y., Lipponen, A., Nordling, K., Hyvärinen, O., Ruosteenoja, K., et al. (2022). The Arctic has warmed nearly four times faster than the globe since 1979. *Communications Earth & Environment*, 3(1), 168. <https://doi.org/10.1038/s43247-022-00498-3>

Raynolds, M. K., Walker, D. A., Balser, A., Bay, C., Campbell, M., Chersov, M. M., et al. (2019). A raster version of the circumpolar arctic vegetation map (CAVM). *Remote Sensing of Environment*, 232, 111297. <https://doi.org/10.1016/j.rse.2019.111297>

Reichstein, M., Bahn, M., Ciais, P., Frank, D., Mahecha, M. D., Seneviratne, S. I., et al. (2013). Climate extremes and the carbon cycle. *Nature*, 500(7462), 287–295. <https://doi.org/10.1038/nature12350>

Reid, K. A., Reid, D. G., & Brown, C. D. (2022). Patterns of vegetation change in Yukon: Recent findings and future research in dynamic subarctic ecosystems. *Environmental Reviews*, 30(3), 380–401. <https://doi.org/10.1139/er-2021-0110>

Romanovsky, V. E., & Osterkamp, T. E. (2000). Effects of unfrozen water on heat and mass transport processes in the active layer and permafrost. *Permafrost and Periglacial Processes*, 11(3), 219–239. [https://doi.org/10.1002/1099-1530\(200007/09\)11:3<219::aid-ppp352>3.0.co;2-7](https://doi.org/10.1002/1099-1530(200007/09)11:3<219::aid-ppp352>3.0.co;2-7)

Rößger, N., Sachs, T., Wille, C., Boike, J., & Kutzbach, L. (2022). Seasonal increase of methane emissions linked to warming in Siberian tundra. *Nature Climate Change*, 12(11), 1031–1036. <https://doi.org/10.1038/s41558-022-01512-4>

Ruess, R. W., Winton, L. M., & Adams, G. C. (2021). Widespread mortality of trembling aspen (*Populus tremuloides*) throughout interior Alaskan boreal forests resulting from a novel cancer disease. *Plos One*, 16(4), e0250078. <https://doi.org/10.1371/journal.pone.0250078>

Salmon, V. G., Soucy, P., Mauritz, M., Celis, G., Natali, S. M., Mack, M. C., & Schuur, E. A. (2016). Nitrogen availability increases in a tundra ecosystem during five years of experimental permafrost thaw. *Global Change Biology*, 22(5), 1927–1941. <https://doi.org/10.1111/gcb.13204>

Saunois, M., Stavert, A. R., Poulter, B., Bousquet, P., Canadell, J. G., Jackson, R. B., et al. (2020). The global methane budget 2000–2017. *Earth System Science Data*, 12(3), 1561–1623. <https://doi.org/10.5194/essd-12-1561-2020>

Schädel, C., Bader, M. K. F., Schuur, E. A. G., Biasi, C., Bracho, R., Capek, P., et al. (2016). Potential carbon emissions dominated by carbon dioxide from thawed permafrost soils. *Nature Climate Change*, 6(10), 950–953. <https://doi.org/10.1038/nclimate3054>

Schaefer, K., Lantuit, H., Romanovsky, V. E., Schuur, E. A., & Witt, R. (2014). The impact of the permafrost carbon feedback on global climate. *Environmental Research Letters*, 9(8), 085003. <https://doi.org/10.1088/1748-9326/9/8/085003>

Scholten, R. C., Jandt, R., Miller, E. A., Rogers, B. M., & Veraverbeke, S. (2021). Overwintering fires in boreal forests. *Nature*, 593(7859), 399–404. <https://doi.org/10.1038/s41586-021-03437-y>

Schuur, E. A. G., Abbott, B. W., Commane, R., Ernakovich, J., Euskirchen, E., Hugelius, G., et al. (2022). Permafrost and climate change: Carbon cycle feedbacks from the warming arctic. *Annual Review of Environment and Resources*, 47(1), 343–371. <https://doi.org/10.1146/annurev-environ-012220-011847>

Schuur, E. A. G., Bockheim, J., Canadell, J. G., Euskirchen, E., Field, C. B., Goryachkin, S. V., et al. (2008). Vulnerability of permafrost carbon to climate change: Implications for the global carbon cycle. *Bioscience*, 58(8), 701–714. <https://doi.org/10.1641/b580807>

Schuur, E. A. G., Bracho, R., Celis, G., Belshe, E. F., Ebert, C., Ledman, J., et al. (2021). Tundra underlain by thawing permafrost persistently emits carbon to the atmosphere over 15 years of measurements. *Journal of Geophysical Research-Biogeosciences*, 126(6). <https://doi.org/10.1029/2020JG006044>

Schuur, E. A. G., McGuire, A. D., Schädel, C., Grosse, G., Harden, J. W., Hayes, D. J., et al. (2015). Climate change and the permafrost carbon feedback. *Nature*, 520(7546), 171–179. <https://doi.org/10.1038/nature14338>

Schuur, E. A. G., Vogel, J. G., Crummer, K. G., Lee, H., Sickman, J. O., & Osterkamp, T. E. (2009). The effect of permafrost thaw on old carbon release and net carbon exchange from tundra. *Nature*, 459(7246), 556–559. <https://doi.org/10.1038/nature08031>

Schwalm, C. R., Schaefer, K., Fisher, J. B., Huntzinger, D., Elshorbany, Y., Fang, Y., et al. (2019). Divergence in land surface modeling: Linking spread to structure. *Environmental Research Communications*, 1(11), 111004. <https://doi.org/10.1088/2515-7620/ab4a8a>

Segers, R. (1998). Methane production and methane consumption: A review of processes underlying wetland methane fluxes. *Biogeochemistry*, 41(1), 23–51. <https://doi.org/10.1023/a:1005929032764>

Shaver, G. R., Billings, W. D., Chapin, F. S., Giblin, A. E., Nadelhoffer, K. J., Oechel, W. C., & Rastetter, E. B. (1992). Global change and the carbon balance of arctic ecosystems. *Bioscience*, 42(6), 433–441. <https://doi.org/10.2307/1311862>

Shevtsova, I., Heim, B., Kruse, S., Schroder, J., Troeva, E. I., Pestryakova, L. A., et al. (2020). Strong shrub expansion in tundra-taiga, tree infilling in taiga and stable tundra in central Chukotka (north-eastern Siberia) between 2000 and 2017. *Environmental Research Letters*, 15(8), 085006. <https://doi.org/10.1088/1748-9326/ab9059>

Shi, Z., Allison, S. D., He, Y., Levine, P. A., Hoyt, A. M., Beem-Miller, J., et al. (2020). The age distribution of global soil carbon inferred from radiocarbon measurements. *Nature Geoscience*, 13(8), 555–559. <https://doi.org/10.1038/s41561-020-0596-z>

Shur, Y. L., Hinkel, K. M., & Nelson, F. E. (2005). The transient layer: Implications for geocryology and climate-change science. *Permafrost and Periglacial Processes*, 16(1), 5–17. <https://doi.org/10.1002/ppp.518>

Shur, Y. L., & Jorgenson, M. T. (2007). Patterns of permafrost formation and degradation in relation to climate and ecosystems. *Permafrost and Periglacial Processes*, 18(1), 7–19. <https://doi.org/10.1002/ppp.582>

Sistla, S. A., Moore, J. C., Simpson, R. T., Gough, L., Shaver, G. R., & Schimel, J. P. (2013). Long-term warming restructures Arctic tundra without changing net soil carbon storage. *Nature*, 497(7451), 615–618. <https://doi.org/10.1038/nature12129>

Sitch, S., Friedlingstein, P., Gruber, N., Jones, S. D., Murray-Tortarolo, G., Ahlström, A., et al. (2015). Recent trends and drivers of regional sources and sinks of carbon dioxide. *Biogeosciences*, 12(3), 653–679. <https://doi.org/10.5194/bg-12-653-2015>

Sjöberg, Y., Siewert, M. B., Rudy, A. C. A., Paquette, M., Bouchard, F., Malenfant-Lepage, J., & Fritz, M. (2020). Hot trends and impact in permafrost science. *Permafrost and Periglacial Processes*, 31(4), 461–471. <https://doi.org/10.1002/ppp.2047>

Smith, N. D., Burke, E. J., Schanke Aas, K., Althuizen, I. H. J., Boike, J., Christiansen, C. T., et al. (2022). Explicitly modelling microtopography in permafrost landscapes in a land surface model (JULES vn5.4\_microtopography). *Geoscientific Model Development*, 15(9), 3603–3639. <https://doi.org/10.5194/gmd-15-3603-2022>

Smith, S. L., O'Neill, H. B., Isaksen, K., Noetzli, J., & Romanovsky, V. E. (2022). The changing thermal state of permafrost. *Nature Reviews Earth & Environment*, 3(1), 10–23. <https://doi.org/10.1038/s43017-021-00240-1>

Song, X., Wang, D.-Y., Li, F., & Zeng, X.-D. (2021). Evaluating the performance of CMIP6 Earth system models in simulating global vegetation structure and distribution. *Advances in Climate Change Research*, 12(4), 584–595. <https://doi.org/10.1016/j.accre.2021.06.008>

Stofferahn, E., Fisher, J. B., Hayes, D. J., Schwalm, C. R., Huntzinger, D. N., Hanton, W., et al. (2019). The Arctic-Boreal vulnerability experiment model benchmarking system. *Environmental Research Letters*, 14(5), 055002. <https://doi.org/10.1088/1748-9326/ab10fa>

Strack, M., Hayne, S., Lovitt, J., McDermid, G. J., Rahman, M. M., Saraswati, S., & Xu, B. (2019). Petroleum exploration increases methane emissions from northern peatlands. *Nature Communications*, 10(1), 2804. <https://doi.org/10.1038/s41467-019-10762-4>

Strauss, J., Laboor, S., Schirrmeyer, L., Fedorov, A. N., Fortier, D., Froese, D., et al. (2021). Circum-Arctic map of the Yedoma permafrost domain. *Frontiers in Earth Science*, 9. <https://doi.org/10.3389/feart.2021.758360>

Strauss, J., Laboor, S., Schirrmeyer, L., Fedorov, A. N., Fortier, D., Froese, D. G., et al. (2022). Database of ice-rich Yedoma permafrost version 2 (IRYP v2). *PANGAEA*. <https://doi.org/10.1594/PANGAEA.940078>

Strauss, J., Schirrmeyer, L., Grosse, G., Fortier, D., Hugelius, G., Knoblauch, C., et al. (2017). Deep Yedoma permafrost: A synthesis of depositional characteristics and carbon vulnerability. *Earth-Science Reviews*, 172, 75–86. <https://doi.org/10.1016/j.earscirev.2017.07.007>

Sturm, M., Schimel, J., Michaelson, G., Welker, J. M., Oberbauer, S. F., Liston, G. E., et al. (2005). Winter biological processes could help convert arctic tundra to shrubland. *Bioscience*, 55(1), 17–26. [https://doi.org/10.1641/0006-3568\(2005\)055\[0017:wbpchc\]2.0.co;2](https://doi.org/10.1641/0006-3568(2005)055[0017:wbpchc]2.0.co;2)

Sweeney, C., Dlugokencky, E., Miller, C. E., Wofsy, S., Karion, A., Dinardo, S., et al. (2016). No significant increase in long-term CH<sub>4</sub> emissions on North Slope of Alaska despite significant increase in air temperature. *Geophysical Research Letters*, 43(12), 6604–6611. <https://doi.org/10.1002/2016GL069292>

Tank, S. E., Vonk, J. E., Walvoord, M. A., McClelland, J. W., Laurion, I., & Abbott, B. W. (2020). Landscape matters: Predicting the biogeochemical effects of permafrost thaw on aquatic networks with a state factor approach. *Permafrost and Periglacial Processes*, 31(3), 358–370. <https://doi.org/10.1002/ppp.2057>

Tarnocai, C., Canadell, J. G., Schuur, E. A. G., Kuhry, P., Mazzhitova, G., & Zimov, S. (2009). Soil organic carbon pools in the northern circumpolar permafrost region. *Global Biogeochemical Cycles*, 23(2), GB2023. <https://doi.org/10.1029/2008gb003327>

Thornton, B. F., Wik, M., & Crill, P. M. (2016). Double-counting challenges the accuracy of high-latitude methane inventories. *Geophysical Research Letters*, 43(24), 12569–12577. <https://doi.org/10.1002/2016gl071772>

Treat, C. C., Bloom, A. A., & Marushchak, M. E. (2018b). Non-growing season methane emissions—A significant component of annual emissions across northern ecosystems. *Global Change Biology*, 24(8), 3331–3343. <https://doi.org/10.1111/gcb.14137>

Treat, C. C., Bloom, A. A., & Marushchak Maija, E. (2018a). Cumulative growing season, non-growing season, and annual methane fluxes from temperate, boreal, and tundra wetlands and uplands [Dataset]. *PANGAEA*. <https://doi.org/10.1594/PANGAEA.886976>

Treat, C. C., Jones, M. C., Alder, J., Sannel, A. B. K., Camill, P., & Frolking, S. (2021). Predicted vulnerability of carbon in permafrost peatlands with future climate change and permafrost thaw in western Canada. *Journal of Geophysical Research: Biogeosciences*, e2020JG005872. <https://doi.org/10.1029/2020JG005872>

Treat, C. C., Jones, M. C., Camill, P., Gallego-Sala, A., Garneau, M., Harden, J. W., et al. (2016). Effects of permafrost aggradation on peat properties as determined from a pan-Arctic synthesis of plant macrofossils. *Journal of Geophysical Research: Biogeosciences*, 121(1), 78–94. <https://doi.org/10.1002/2015JG003061>

Treat, C. C., Kleinen, T., Broothaerts, N., Dalton, A. S., Dommain, R., Douglas, T. A., et al. (2019). Widespread global peatland establishment and persistence over the last 130,000 y. *Proceedings of the National Academy of Sciences U.S.A.*, 116(4827). 201813305. <https://doi.org/10.1073/pnas.1813305116>

Treat, C. C., Natali, S. M., Ernakovich, J., Iversen, C. M., Lupascu, M., McGuire, A. D., et al. (2015). A pan-Arctic synthesis of CH<sub>4</sub> and CO<sub>2</sub> production from anoxic soil incubations. *Global Change Biology*, 21(7), 2787–2803. <https://doi.org/10.1111/gcb.12875>

Treharne, R., Bjerke, J. W., Tømmervik, H., Stendardi, L., & Phoenix, G. K. (2019). Arctic browning: Impacts of extreme climatic events on heathland ecosystem CO<sub>2</sub> fluxes. *Global Change Biology*, 25(2), 489–503. <https://doi.org/10.1111/gcb.14500>

Tsuruta, A., Kivimäki, E., Lindqvist, H., Karppinen, T., Backman, L., Hakkarainen, J., et al. (2023). CH<sub>4</sub> fluxes derived from assimilation of TROPOMI XCH<sub>4</sub> in carbontracker Europe-CH4: Evaluation of seasonality and spatial distribution in the northern high latitudes. *Remote Sensing*, 15(6), 1620. <https://doi.org/10.3390/rs15061620>

Turetsky, M. R., Abbott, B. W., Jones, M. C., Anthony, K. W., Olefeldt, D., Schuur, E. A. G., et al. (2020). Carbon release through abrupt permafrost thaw. *Nature Geoscience*, 13(2), 138–143. <https://doi.org/10.1038/s41561-019-0526-0>

Turetsky, M. R., Kotowska, A., Bubier, J., Duse, N. B., Crill, P., Hornbrook, E. R. C., et al. (2014). A synthesis of methane emissions from 71 northern, temperate, and subtropical wetlands. *Global Change Biology*, 20(7), 2183–2197. <https://doi.org/10.1111/gcb.12580>

Ueyama, M., Iwata, H., Nagano, H., Tahara, N., Iwama, C., & Harazono, Y. (2019). Carbon dioxide balance in early-successional forests after forest fires in interior Alaska. *Agricultural and Forest Meteorology*, 275, 196–207. <https://doi.org/10.1016/j.agrformet.2019.05.020>

Van Wees, D., Van Der Werf, G. R., Randerson, J. T., Rogers, B. M., Chen, Y., Veraverbeke, S., et al. (2022). Global biomass burning fuel consumption and emissions at 500m spatial resolution based on the Global Fire Emissions Database (GFED). *Geoscientific Model Development*, 15(22), 8411–8437. <https://doi.org/10.5194/gmd-15-8411-2022>

Varner, R. K., Crill, P. M., Frolking, S., McCalley, C. K., Burke, S. A., Chanton, J. P., et al. (2022). Permafrost thaw driven changes in hydrology and vegetation cover increase trace gas emissions and climate forcing in Stordalen Mire from 1970 to 2014. *Philosophical Transactions of the Royal Society a-Mathematical Physical and Engineering Sciences*, 380(2215). <https://doi.org/10.1098/rsta.2021.0022>

Varney, R. M., Chadburn, S. E., Burke, E. J., & Cox, P. M. (2022). Evaluation of soil carbon simulation in CMIP6 Earth system models. *Bio-geosciences*, 19(19), 4671–4704. <https://doi.org/10.5194/bg-19-4671-2022>

Veraverbeke, S., Delcourt, C. J. F., Kukavskaya, E., Mack, M., Walker, X., Hesselt, T., et al. (2021). Direct and longer-term carbon emissions from arctic-boreal fires: A short review of recent advances. *Current Opinion in Environmental Science & Health*, 23, 100277. <https://doi.org/10.1016/j.coesh.2021.100277>

Virkkala, A. M., Aalto, J., Rogers, B. M., Tagesson, T., Treat, C. C., Natali, S. M., et al. (2021b). Data for: "Statistical upscaling of ecosystem CO<sub>2</sub> fluxes across the terrestrial tundra and boreal domain: Regional patterns and uncertainties" [Dataset]. Zenodo. <https://doi.org/10.5281/zenodo.4519583>

Virkkala, A. M., Aalto, J., Rogers, B. M., Tagesson, T., Treat, C. C., Natali, S. M., et al. (2021a). Statistical upscaling of ecosystem CO<sub>2</sub> fluxes across the terrestrial tundra and boreal domain: Regional patterns and uncertainties. *Global Change Biology*, 27(17), 4040–4059. <https://doi.org/10.1111/gcb.15659>

Virkkala, A. M., Natali, S., Rogers, B. M., Watts, J. D., Savage, K., Connan, S. J., et al. (2021c). The ABCflux database: Arctic-boreal CO<sub>2</sub> flux and site environmental data, 1989–2020 [Dataset]. ORNL Distributed Active Archive Center. <https://doi.org/10.3334/ORNLDAA/1934>

Virkkala, A. M., Natali, S. M., Rogers, B. M., Watts, J. D., Savage, K., Connan, S. J., et al. (2022). The ABCflux database: Arctic-boreal CO<sub>2</sub> flux observations and ancillary information aggregated to monthly time steps across terrestrial ecosystems. *Earth System Science Data*, 14(1), 179–208. <https://doi.org/10.5194/essd-14-179-2022>

Virkkala, A. M., Virtanen, T., Lehtonen, A., Rinne, J., & Luoto, M. (2018). The current state of CO<sub>2</sub> flux chamber studies in the arctic tundra: A review. *Progress in Physical Geography-Earth and Environment*, 42(2), 162–184. <https://doi.org/10.1177/0309133317745784>

Vitt, D. H., Halsey, L. A., & Zoltai, S. C. (2000). The changing landscape of Canada's western boreal forest: The current dynamics of permafrost. *Canadian Journal of Forest Research-Revue Canadienne De Recherche Forestiere*, 30(2), 283–287. <https://doi.org/10.1139/cjfr-30-2-283>

Voigt, C., Virkkala, A.-M., Hould Gosselin, G., Bennett, K. A., Black, T. A., Dett, M., et al. (2023). Arctic soil methane sink increases with drier conditions and higher ecosystem respiration. *Nature Climate Change*, 13(10), 1095–1104. <https://doi.org/10.1038/s41558-023-01785-3>

Vonk, J. E., Tank, S. E., Bowden, W. B., Laurion, I., Vincent, W. F., Alekseychik, P., et al. (2015). Reviews and syntheses: Effects of permafrost thaw on Arctic aquatic ecosystems. *Biogeosciences*, 12(23), 7129–7167. <https://doi.org/10.5194/bg-12-7129-2015>

Vonk, J. E., Tank, S. E., & Walvoord, M. A. (2019). Integrating hydrology and biogeochemistry across frozen landscapes. *Nature Communications*, 10(1), 5377. <https://doi.org/10.1038/s41467-019-13361-5>

Walker, D. A., Raynolds, M. K., Daniëls, F. J. A., Einarsson, E., Elvebakk, A., Gould, W. A., et al. (2005). The Circumpolar Arctic vegetation map. *Journal of Vegetation Science*, 16(3), 267–282. <https://doi.org/10.1111/j.1654-1103.2005.tb02365.x>

Walker, H. J. (1998). Arctic deltas. *Journal of Coastal Research*, 14(3), 719–738.

Walker, X. J., Baltzer, J. L., Cumming, S. G., Day, N. J., Ebert, C., Goetz, S., et al. (2019). Increasing wildfires threaten historic carbon sink of boreal forest soils. *Nature*, 572(7770), 520–523. <https://doi.org/10.1038/s41586-019-1474-y>

Walter Anthony, K. M., Anthony, P., Grosse, G., & Chanton, J. (2012). Geologic methane seeps along boundaries of Arctic permafrost thaw and melting glaciers. *Nature Geoscience*, 5(6), 419–426. <https://doi.org/10.1038/geo1480>

Walter Anthony, K. M., Zimov, S. A., Grosse, G., Jones, M. C., Anthony, P. M., Iii, F. S. C., et al. (2014). A shift of thermokarst lakes from carbon sources to sinks during the Holocene epoch. *Nature*, 511(7510), 452–456. <https://doi.org/10.1038/nature13560>

Wang, J. A., Sulla-Menashe, D., Woodcock, C. E., Sonnentag, O., Keeling, R. F., & Friedl, M. A. (2020). Extensive land cover change across Arctic–Boreal Northwestern North America from disturbance and climate forcing. *Global Change Biology*, 26(2), 807–822. <https://doi.org/10.1111/gcb.14804>

Ward Jones, M. K., Schwoerer, T., Gannon, G. M., Jones, B. M., Kanevskiy, M. Z., Sutton, I., et al. (2022). Climate-driven expansion of northern agriculture must consider permafrost. *Nature Climate Change*, 12(8), 699–703. <https://doi.org/10.1038/s41558-022-01436-z>

Watts, J. D., Farina, M., Kimball, J. S., Schiferl, L. D., Liu, Z. H., Arndt, K. A., et al. (2023). Carbon uptake in Eurasian boreal forests dominates the high-latitude net ecosystem carbon budget. *Global Change Biology*, 29(7), 1870–1889. <https://doi.org/10.1111/gcb.16553>

Watts, J. D., Natali, S. M., Minions, C., Risk, D., Arndt, K., Zona, D., et al. (2021). Soil respiration strongly offsets carbon uptake in Alaska and Northwest Canada. *Environmental Research Letters*, 16(8), 084051. <https://doi.org/10.1088/1748-9326/ac1222>

Webster, K. L., Bhatti, J. S., Thompson, D. K., Nelson, S. A., Shaw, C. H., Bona, K. A., et al. (2018). Spatially-integrated estimates of net ecosystem exchange and methane fluxes from Canadian peatlands. *Carbon Balance and Management*, 13(1), 16. <https://doi.org/10.1186/s13021-018-0105-5>

Whalen, S. C. (2005). Biogeochemistry of methane exchange between natural wetlands and the atmosphere. *Environmental Engineering Science*, 22(1), 73–94. <https://doi.org/10.1089/ees.2005.22.73>

Wik, M., Varner, R. K., Anthony, K. W., MacIntyre, S., & Bastviken, D. (2016). Climate-sensitive northern lakes and ponds are critical components of methane release. *Nature Geoscience*, 9(2), 99–105. <https://doi.org/10.1038/geo2578>

Xu, X., Riley, W. J., Koven, C. D., Billesbach, D. P., Chang, R. Y. W., Commane, R., et al. (2016). A multi-scale comparison of modeled and observed seasonal methane emissions in northern wetlands. *Biogeosciences*, 13(17), 5043–5056. <https://doi.org/10.5194/bg-13-5043-2016>

Xu, X., Riley, W. J., Koven, C. D., & Jia, G. (2018). Observed and simulated sensitivities of spring greenup to preseason climate in northern temperate and boreal regions. *Journal of Geophysical Research: Biogeosciences*, 123(1), 60–78. <https://doi.org/10.1002/2017JG004117>

Xu, X., Yuan, F., Hanson, P. J., Wullschleger, S. D., Thornton, P. E., Riley, W. J., et al. (2016). Reviews and syntheses: Four decades of modeling methane cycling in terrestrial ecosystems. *Biogeosciences*, 13(12), 3735–3755. <https://doi.org/10.5194/bg-13-3735-2016>

Yang, M., Nelson, F. E., Shiklomanov, N. I., Guo, D., & Wan, G. (2010). Permafrost degradation and its environmental effects on the Tibetan plateau: A review of recent research. *Earth-Science Reviews*, 103(1), 31–44. <https://doi.org/10.1016/j.earscirev.2010.07.002>

Yu, Z., Loisel, J., Brousseau, D. P., Beilman, D. W., & Hunt, S. J. (2010). Global peatland dynamics since the last glacial maximum. *Geophysical Research Letters*, 37(13), L13402. <https://doi.org/10.1029/2010gl043584>

Zaehle, S., Jones, C. D., Houlton, B., Lamarque, J.-F., & Robertson, E. (2015). Nitrogen availability reduces CMIP5 projections of twenty-first-century land carbon uptake. *Journal of Climate*, 28(6), 2494–2511. <https://doi.org/10.1175/JCLI-D-13-00776.1>

Zhang, Z., Fluet-Chouinard, E., Jensen, K., McDonald, K., Hugelius, G., Gumbrecht, T., et al. (2021). Development of the global dataset of wetland area and dynamics for methane modeling (WAD2M). *Earth System Science Data*, 13(5), 2001–2023. <https://doi.org/10.5194/essd-13-2001-2021>

Zhang, Z., Poulter, B., Feldman, A. F., Ying, Q., Cais, P., Peng, S., & Li, X. (2023). Recent intensification of wetland methane feedback. *Nature Climate Change*, 13(5), 430–433. <https://doi.org/10.1038/s41558-023-01629-0>

Zimov, N. S., Zimov, S. A., Zimova, A. E., Zimova, G. M., Chuprnyin, V. I., & Chapin, F. S., III. (2009). Carbon storage in permafrost and soils of the mammoth tundra-steppe biome: Role in the global carbon budget. *Geophysics Research Letter*, 36(2). <https://doi.org/10.1029/2008gl036332>

Zolkos, S., Tank, S. E., Kokelj, S. V., Striegl, R. G., Shakil, S., Voigt, C., et al. (2022). Permafrost landscape history shapes fluvial chemistry, ecosystem carbon balance, and potential trajectories of future change. *Global Biogeochemical Cycles*, 36(9), e2022GB007403. <https://doi.org/10.1029/2022GB007403>

Zona, D., Gioli, B., Commane, R., Lindaas, J., Wofsy, S. C., Miller, C. E., et al. (2016). Cold season emissions dominate the Arctic tundra methane budget. *Proceedings of the National Academy of Sciences*, 113(1), 40–45. <https://doi.org/10.1073/pnas.1516017113>

## References From the Supporting Information

Dinerstein, E., Olson, D., Joshi, A., Vynne, C., Burgess, N. D., Wikramanayake, E., et al. (2017). An ecoregion-based approach to protecting half the terrestrial realm. *Bioscience*, 67(6), 534–545. <https://doi.org/10.1093/biosci/bix014>